ALMA MATER STUDIORUM – UNIVERSITÀ DI BOLOGNA

CAMPUS DI CESENA

SCUOLA DI INGEGNERIA E ARCHITETTURA

CORSO DI LAUREA MAGISTRALE IN INGEGNERIA BIOMEDICA

Titolo della tesi

"Analysis of electroencephalography signals collected in a magnetic resonance environment: characterisation of the ballistocardiographic artefact"

Tesi in Bioimmagini LM

Relatore

Prof.ssa Cristiana Corsi

Correlatori

Prof. Dante Mantini

Ing. Marco Marino

Presentata da

Mariangela Del Castello

Anno Accademico 2015/2016

III sessione

Table of contents

Abstract

Simultaneous recording of electroencephalography (EEG) signals and functional magnetic resonance (fMRI) imaging is a powerful approach in the field of neuroscience to study brain functions and dysfunctions. It allows obtaining information about brain functioning with high temporal resolution and high spatial resolution at the same time. The EEG technique records electrical signals of brain activity with a resolution of milliseconds. The fMRI acquisitions give information about the anatomy and the physiology of the brain with a resolution of millimeters.

However, the combination of these two procedures increases the presence of artefacts in the EEG signal, thus obscuring the brain activity. The artefacts are caused by the interactions between the subject, the EEG system and the scanner's magnetic fields. The main two artefacts are: the imaging artefact and the ballistocardiographic (BCG) artefact. The imaging artefact is caused by the gradients switching during the images acquisition. However well-performing methods for its removal have been implemented.

The BCG artefact is related to the cardiac activity of the subject and it is characterized by high variability between each occurrence. The variability is in terms of: amplitude, waveform and duration of the artefact. Several algorithms have been implemented to remove the artefact. However, because of its complex nature, the total removal of the BCG is still a challenging task.

The topic of the thesis is to analyze EEG signals collected in a magnetic resonance environment and to characterize the BCG artefact. The aim is to understand additional features about it that can help to improve or create new methods.

With this work we have shown why the methods proposed in literature can lead to residual artefact in the clean EEG signal. Performing statistical analysis and using statistical tools like Pearson'correlation coefficient, we have found that the BCG artefact occurrences are characterized by a variable delay from the related R peak in the ECG, that is the referring event in cardiac activity in our analysis. Furthermore the R-BCG delay is related to the cardiac frequency: when the cardiac frequency decreases the BCG artefact appears with a larger delay after the R wave. Other findings are about the main contributions to the BCG artefact. Performing the principal component analysis on the average artefact activity across subjects, we have shown that the artefact is due to two principal contributions related to the blood flow in head vessels and its pulsatility in the major arteries in the scalp.

Abstract – Italian version

L'acquisizione simultanea di segnali elettroencefalografici (EEG) e immagini di risonanza magnetica funzionale (fMRI) permette di investigare connessioni e attivazioni cerebrali in modo non invasivo. Inoltre le informazioni ottenute sono caratterizzate da elevata risoluzione temporale ed elevata risoluzione spaziale. La tecnica EEG consente di registrare i potenziali elettrici provenienti dal cervello con una risoluzione temporale dell'ordine del millisecondo. L'fMRI consente di acquisire immagini descriventi anatomia e fisiologia del cervello, con una risoluzione spaziale dell'ordine del millimetro.

Allo stesso tempo però, la presenza del campo magnetico altera in modo non trascurabile la qualità dei segnali EEG acquisiti. In particolare due artefatti sono stati individuati: l'artefatto da gradiente e l'artefatto da ballistocardiogramma (BCG). L'artefatto da gradiente è causato dalla variazione dei gradienti utilizzati per la formazione delle immagini. Grazie alle sue proprietà stazionarie, l'artefatto viene rimosso in maniera efficace dagli algoritmi finora implementati.

L'artefatto da BCG è legato all'attività cardiaca del soggetto, ed è caratterizzato da elevata variabilità tra un'occorrenza e l'altra. La variabilità è in termini di: ampiezza, forma d'onda e durata dell'artefatto. Differenti algoritmi sono stati implementati al fine di rimuoverlo, ma la rimozione completa rimane ancora un difficile obiettivo da raggiungere a causa della sua complessa natura.

L'argomento della tesi riguarda l'analisi di segnali EEG acquisiti in ambiente di risonanza magnetica e la caratterizzazione dell'artefatto BCG. L'obiettivo è individuare ulteriori caratteristiche dell'artefatto che possano condurre al miglioramento dei precedenti metodi, o all'implementazione di nuovi.

Con questa tesi abbiamo mostrato quali sono i motivi che causano la presenza di residui artefattuali nei segnali EEG processati con i metodi presenti in letteratura. Attraverso analisi statistica, usando strumenti come il coefficiente di correlazione di Pearson, abbiamo riscontrato che occorrenze dell'artefatto BCG sono caratterizzate da un ritardo variabile rispetto al picco R sull'ECG, che nella nostra analisi rappresenta l'evento di riferimento nell'attività cardiaca. Abbiamo inoltre trovato che il ritardo R-BCG è legato alla frequenza cardiaca: quando la frequenza cardiaca diminuisce, l'artefatto BCG si presenta con un ritardo maggiore rispetto l'onda R. Le successive valutazioni riguardano i maggiori contributi all'artefatto BCG. Attraverso l'analisi alle componenti principali, eseguita sull'attività media dell'artefatto individuata a seguito di un'analisi inter-subjects. Abbiamo mostrato che l'artefatto è causato da due contributi principali, legati al fluire del sangue dal cuore verso il cervello e alla sua pulsatilità nei vasi principali dello scalpo.

Introduction

The combination of electroencephalography (EEG) technique and functional magnetic resonance imaging (fMRI) is a powerful tool for non-invasive investigation of brain function and dysfunction in presence of diseases. By using these two techniques simultaneously, it is possible to obtain information on brain activity characterized by high temporal resolution (from EEG) and high spatial resolution (from fMRI).

On the other hand, EEG signals recorded in magnetic environment are corrupted by artefactual contributions caused by the interaction between the subject, the EEG electrode assembly and the scanner's magnetic fields. The two main artefacts are: the imaging artefact and the ballistocardiographic (BCG) artefact. The first artefact is caused by the gradients switching during the images acquisition. It is characterized by periodical and consistent occurrences, with amplitude much higher than the EEG signals. The second one is related to the cardiac activity, thus it can be identified using an ECG trace, which is recorded during the EEG-fMRI acquisition. After a QRS complex it is possible to identify a BCG occurrence in the EEG signals. The BCG artifact is caused by three effects: 1) pulse-driven expansion of the scalp due to the pulsatility of the blood, which is affecting especially the areas in correspondence of the major vessels; 2) pulse-driven rotation of the head due to the axial movement of the body after each cardiac ejection; 3) Hall effect in the head vessels due to the blood flow in the magnetic field [22,23]. The first two effects lead to the electrodes movement which, in the magnetic environment, produces an electromotive force that adds up to the EEG signals. The third contribution leads to a force (identified by Lorentz's rule) that adds up to the EEG signals, too. The BCG artefact is characterized by high variability beat-to-beat in terms of amplitude, waveform and duration and they can vary with different magnetic field strengths. [29]

Several algorithms have been implemented for the offline removal of these artefacts. The most used methods are based on Average Artefact Subtraction (AAS) [30], Optimal Basis Set (OBS) [25] and Independent Component Analysis (ICA) [33, 34]. Each of these methods makes assumptions which cannot be easily satisfied since the BCG artefact has non–stationary features. For example the AAS and OBS based methods hypothesize that the delay between the BCG occurrence and the R peak in the ECG is constant. Whereas the ICA procedure is based on the assumption that the sources are stationary, while the BCG artefact is not stationary. Thus removing the artefact it is still a challenging task.

The purpose of this thesis is to analyze EEG signals recorded in a scanner for MR imaging. Focusing especially on BCG artefact occurrences, with the aim to better characterize the artefact and to understand why the implemented methods can lead to artefact residual.
The analysis was performed using functions implemented in MATLAB and in the EEGLab toolbox.
The work has been conducted with the BIND (Brain Imaging & Neural Dynamics) group at the KU Leuven University in Belgium.
The thesis is composed by four main chapters. The first two chapters deal with introductive issues on EEG, fMRI and related artefacts. They will be useful for a deeper understanding of methods and obtained results which are reported in the third and fourth chapters.
Specifically, the first chapter is an overview about the EEG and MRI techniques, the EEG instrumentation and the MRI acquisition system. Main concepts about EEG-fMRI approach are discussed. Furthermore, a brief description of EEG instrumentation for magnetic environment and the protocol for EEG-fMRI acquisition are reported.
The second chapter deals with artefacts and it is divided in two parts. In the first one the imaging artefact and the methods implemented for its removal are described. The second part is focused on the description of the BCG artefact, its origins and features. Moreover the main implemented methods for removing the BCG artefacts are described (like AAS, OBS, ICA) with a comparison about their performances.
The third chapter is about materials and methods. Information about the experimental EEG-fMRI acquisition, used instrumentation and parameters features is given. The methods used during the EEG signals analysis are described. Specifically, the methods used for imaging artefact removal, pre-processing steps of ECG signals and the concept of signals epoching are reported. Furthermore, statistical analysis tools such as Tukey's method for outlier removal, Pearson's correlation coefficient, and the using of principal components analysis are described.
In the fourth chapter the results obtained using the methods described in the previous chapter are illustrated and discussed.
In the final part conclusion and the future perspective are described.

Enjoy!

Chapter 1 – EEG & MRI techniques

1.1 Electroencephalography EEG

1.1.1 Electrophisiological basis of EEG

Electroencephalography (EEG) is a non-invasive technique that permits to reveal electrical fields produced by neurons. The EEG signal is measured on the scalp and it describes the synchronized activity of cortical neuronal populations.

The cerebral cortex is composed by six functional layers and its neurons can be divided in two groups: pyramidal neurons and non-pyramidal neurons.

Pyramidal neurons can be found in the third, fifth and sixth layers, and they are characterized by: triangular shaped soma with the apex on the top, a single axon, a large apical dendrite, multiple basal dendrites, and dendritic spines. Apical dendrites can usually extend until the superficial layer of the cortex, and they run parallel to each others, while being perpendicular to the cortical surface.

Non-pyramidal neurons are characterized by: a smaller soma compared to pyramidal neurons, short dendrites and a short axon. These neurons are also called local neurons since their axon and dendrites transmit signals only to the neighboring cells (see fig. 1).

The main contribution to the EEG signals comes from pyramidal neurons, due to the apical dendrites organization. The parallelism between apical dendrites and the synchronized activity allow measuring an electrical signal on the scalp.

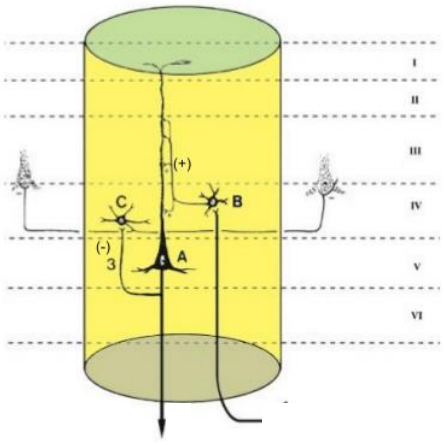

Figure 1 Cortical column with pyramidal (A) and non-pyramidal neurons (B-C). The cortical column is composed by seven layers (indicated by I, II, III, IV, V, VI).

At level of a single neuron, the electrical phenomena are based on the occurrence of ionic currents. There are two forms of neuronal activation: the fast depolarization of the neuronal membranes and the slower changes in membrane potential due to synaptic activation.

The first one results in the generation of an action potential mediated by sodium and potassium voltage-dependent ionic conductances. The action potential generates a rapid change in the membrane potential, that varies from negative to positive while returning to the initial negative value (about -70 mV) in 1-2 ms. In this way, a pulse is generated and it propagates along axons and dendrites without any loss of amplitude.

The second ones are mediated by neurotransmitters and they can be distinguished in two kinds: excitatory postsynaptic potentials (EPSPs) and inhibitory postsynaptic potentials (IPSPs). This type of neuronal activation differs depending on the neurotransmitter and the corresponding receptor. During an EPSP the transmembrane current is generated by positive ions inwards (e.g. Na^+), while during an IPSP the transmembrane current is generated by negative ions inwards (e.g. Cl^-) or positive ions outwards (e.g. K^+). This transmembrane current flows in or out of the neuron in correspondence of the active synaptic sites. It is important to underline that the contribution of action potentials to the signal recorded by EEG instrumentation is very low, as axons do not have a global preferential direction. On the contrary, they have different directions in the cortical space. Furthermore, the brief duration (1-2 ms) of the action potentials does not allow axons to release the signal in synchrony way. On the other hand, the higher duration (10-100 ms) of synaptic currents makes easier to add up the generated potentials even if the synchronization is not perfect. Accordingly, EEG measurements represent the expression of the post-synaptic activities of pyramidal neurons population in the cerebral cortex. [1][2]

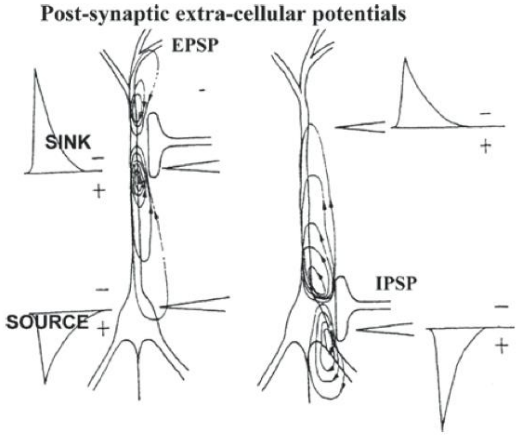

Figure 2 Scheme of cortical pyramidal cell showing the patterns of current flow caused by two modes of synaptic activation at an excitatory (E) and an inhibitory (I) synapse. (Adapted from [1])

EEG recordings show continuous fluctuations in time, which frequency and amplitude are influenced by the internal states of the subject and by the occurrence of external conditions. These fluctuations have been categorized in different groups called rhythms, based on the frequency content. It has been shown that different brain rhythms are associated to the different tasks or states.

Six types of rhythms have been observed.

Delta rhythm (δ): characterized by a frequency range between 0.5 Hz and 4 Hz and amplitude range between 20 μV and 200 μV. It is the slowest rhythm but with the highest amplitude. It is seen normally in babies and in adults during the NON-REM deep sleep.

Theta rhythm (θ): characterized by a frequency range between 4 Hz and 7 Hz and amplitude range between 20 μV and 100 μV. It can be observed especially during the pre-sleep phase.

Alpha rhythm (α): characterized by a frequency range between 8 Hz and 13 Hz and amplitude range between 20 μV and 50 μV. It is seen during conscious relaxed state with closed eyes.

Mu rhythm (μ): characterized by the same frequency range as alpha rhythm, it can be observed during physical rest, but unlike the alpha rhythm, it is seen also with eyes open.

Beta rhythm (β): characterized by a frequency range between 13 Hz and 30 Hz and amplitude range between 5 μV and 30 μV. It can be observed during attention and concentrating state.

Gamma Rhythm (γ) : characterized by frequencies higher then 30 Hz and amplitude range between 1 μV and 20 μV. It can be observed during cognitive function.

In table 1 all the features about brain rhythms are summarized. [2]

Table 1 Main features about brain rhythms

Rhythm	*Frequency (Hz)*	*Amplitude (μV)*	*Brain Location*	*Brain Condition*
δ	0.5 - 4	20 - 200	Frontal and parietal lobe	Non – REM deep sleep; Pathological condition; Coma
θ	4 - 8	20 - 100	Temporal and parietal lobe	Pre-sleep; Non – REM sleep; Memory and learning
α	8 - 13	20 - 50	Occipital and parietal lobe	Conscious relaxed state;

				Closed eyes
μ	8 - 13	20 - 50	Frontal (motor cortex) lobe	Physical rest
β	13 - 30	5 - 30	Parietal and frontal lobe	Active concentration
γ	> 30	1 - 20	Frontal lobe	Perception; attention; Information integration

1.1.2 EEG instrumentation

EEG recording systems usually include a cap with multiple EEG electrodes, an amplifier, and one personal computer for acquisition and visualization (figure 3).

Figure 3 Example of EEG equipment (from the company Electrical Geodesics)

The electrodes are arranged in a cap that provides a partial or full coverage of the scalp, which allows to record signals from different areas of the cortex. EEG sensors can be made with different materials, even if the most used in EEG recordings are made in silver-chloride (AgCl).

In clinical settings, most commonly, EEG caps are composed by a low number of electrodes. Low-density caps were originally composed by 16 or 21 electrodes, but the number of sensors has increased across the years up to 32 and 64 electrodes (see fig.4). In

the recent years, high-density EEG (HD-EEG) caps have become also available, and especially used for research purposes. These caps are composed by 128 or 256 electrodes (see fig.4), which enable to achieve higher accuracy on the source localization of the recorded brain activity [3].

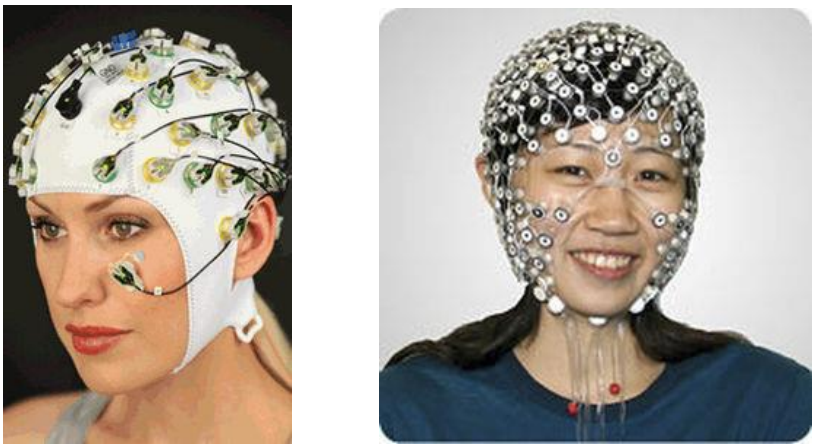

Figure 4 Left: low-density EEG cap with an EOG electrode. Right: high-density EEG net

When the cap is set up on the subject's head, a good contact between the surface of the electrode and the scalp is needed. To achieve it, gel or saline solutions are used to minimize the electrode impedance that can be checked on the monitor of the instrumentation.
The cap can contain also extra electrodes for recording other physiological signal, e.g. electrooculographic (EOG) signal and electrocardiographic signal (ECG).

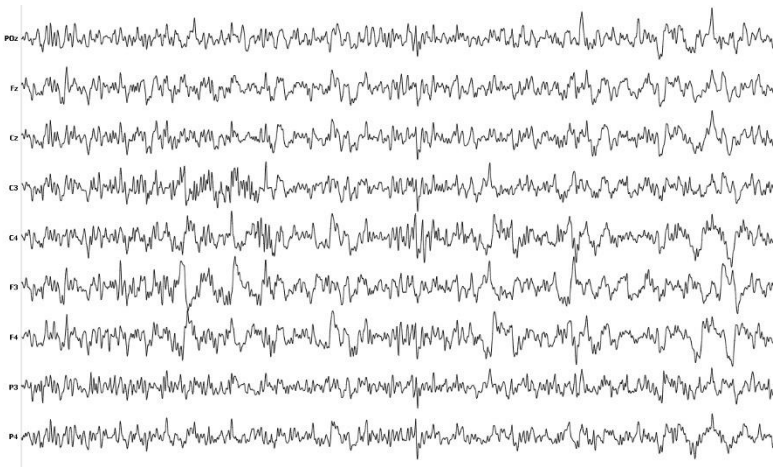

Figura 5 EEG traces recorded by 9 electrodes

The amplitude of electrical activity on the scalp is very low (see table 1) so an amplifier is essential in order to amplify the data and make them readable [2]. By hardware and software equipment, data can be visualized in real time, furthermore initial processing of the signals can be execute, for example notch filtering.
In figure 5 an example of EEG traces is illustrated.

1.2 Magnetic Resonance Imaging – MRI

1.2.1 Fundamental concepts of MRI

The magnetic resonance imaging is an imaging technique, that allows obtaining images of soft tissues in a non-invasive way and without using ionizing radiation.
The human body contains a high percentage of water and, therefore, high quantity of hydrogen atoms. This technique is based on the interaction between tissue's hydrogen atoms and a magnetic field. In particular, the magnetic field $\overrightarrow{B}$ affects the hydrogen atoms' spin. This interaction is described by the magnetic dipole moment $\overrightarrow{\mu}$ of the spin. When spins are in a magnetic environment, they tend to align along the field direction, in a parallel or antiparallel way. The macroscopic magnetization could be described by vector $\overrightarrow{M}$, that expresses the sum of magnetic dipole moments in the considered tissue, and it is parallel to $\overrightarrow{B}$. In the case $\overrightarrow{M}$ is parallel to $\overrightarrow{B}$, the equilibrium condition occurs, but when the protons are exposed to an electromagnetic wave, characterized by a certain frequency, called Larmor frequency, $\overrightarrow{M}$ is tilted proportionally to the exposure duration (see fig. 6). $\overrightarrow{M}$ rotates around the magnetic field vector, trough a movement called precession, while protons release an electromagnetic wave characterized by the Larmor frequency. Successively, the tilted $\overrightarrow{M}$ returns to its original state, this movement is called relaxation. [1]

It is noteworthy that the Larmor frequency is proportional to the static magnetic field and specific for each ionic species, with a value of 42.6 MHz/T for hydrogen atoms. [5]
The Larmor frequency is defined as:

$$f = \frac{\gamma}{2\pi} B \qquad (1)$$

Where γ is the gyromagnetic ratio characterizing the ionic specie, B is the strength of magnetic field.

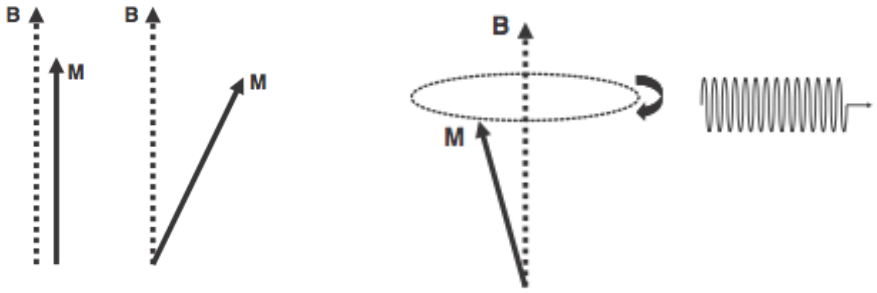

Figure 6 On the left: vector M parallel and tilted to the field B. On the right: tilted M rotating around B sends out an electromagnetic wave (Adapted from [1])

In the next paragraphs, the operating principles of the magnetic resonance imaging technique are sum up.

When the subject lies in the scanner, he is exposed to a strong static magnetic field $\overrightarrow{B}$, which builds up a macroscopic magnetization $\overrightarrow{M}$ parallel to $\overrightarrow{B}$. An electromagnetic wave characterized by protons' Larmor frequency and duration of few milliseconds is transmitted a radiofrequency system. A detector is switched on to recording the signals emitted by the protons.

In order to produce an image, it is necessary to perturb the alignment between the static magnetic field $\overrightarrow{B}$ and protons' spin. Three different gradient fields along three orthogonal directions are generated, with the static magnetic field always present. In this way specific tissue portions will be excited and spatial resolution in the tissue is achieved.

The gradient in the x direction (left/right) is indicated as G_x (see fig. 7). When it is switched on, the magnetic field is modified in a way that it increases linearly in the x direction, so that the electromagnetic wave emitted by protons will have a Larmor frequency that depends on their position. This signal is processed by Fourier Transform to evaluate protons' position from the frequency spectrum.

The second gradient is G_y in y direction (anterior/posterior), perpendicular to x direction, it is switched on when a x-coordinate is already defined (G_x switched on). The starting points of the signals from the anterior and posterior regions are different. They have different phases because they are shifted in time. So it is possible to identify different y coordinates evaluating different phases in the signal (see fig. 8).

In the z direction, that is perpendicular to the previous ones, there is the gradient G_z. It is switched on at the beginning of the experiment, by the transmission of a RF (radiofrequency) pulse (see fig. 9). With this gradient a slice is selected, and the Larmor

frequency is constant in it. So if a RF pulse, characterized by a certain frequency $f_{0,,}$ is sent the magnetization vector will be tilted only in the slice characterized by the a Larmor frequency equal to f_0, while, in the other slices, the Larmor frequencies are higher or lower than f_0. This process is repeated for different values of frequency in order to record multislice images datasets. [1]

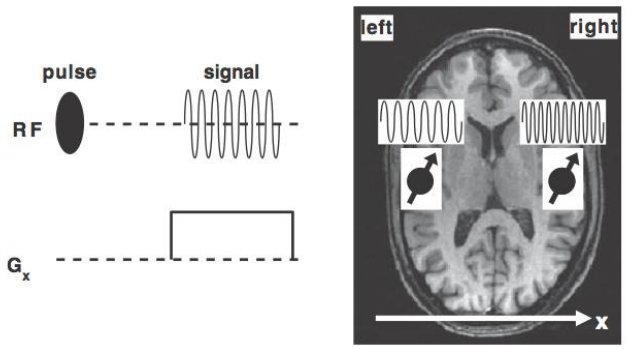

Figure 7 Gradient in x direction for the frequency encoding (Adapted from [1])

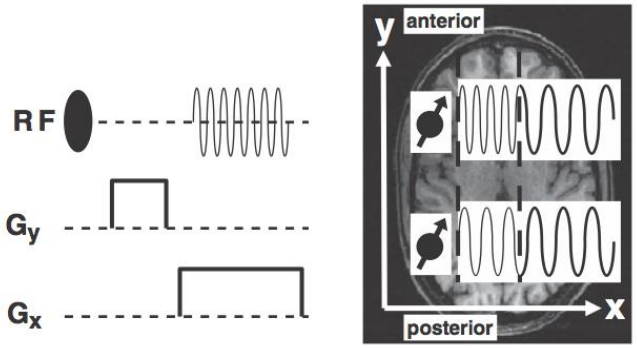

Figure 8 Gradient in y direction with phase encoding (Adapted from [1])

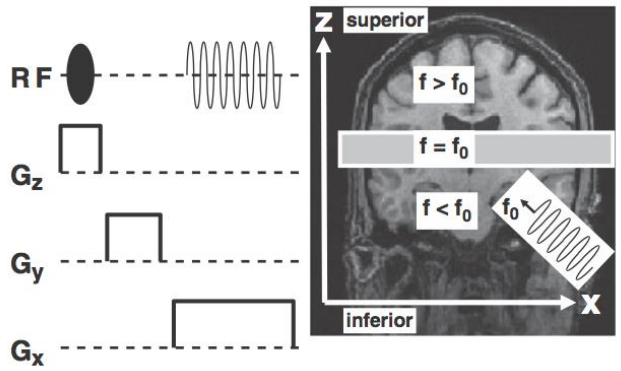

Figure 9 Gradient in z direction for the slice selection (Adapted from [1])

As previously mentioned, the vector $\overrightarrow{M}$ can be tilted by an RF pulse for a limited period and then, during the relaxation, it goes back to the equilibrium state. During the relaxation, the magnetization vector is composed by two components: the longitudinal component, that is parallel to $\overrightarrow{B}$, and the transverse component, that is perpendicular to $\overrightarrow{B}$.

The longitudinal component reaches the maximum value corresponding to the time constant T1, called longitudinal relaxation time, by means of a process called spin-lattice relaxation, in which free water spins transfer energy to the surrounding environment. T1 refers to the mean time for an individual spin to return to its equilibrium state. It increases exponentially until a saturation value.

The transversal component vanishes by following the time constant T2, called transverse relaxation time, which explicates a process called spin-spin relaxation, which is characterized by exchanges of small amounts of energy between free water spins. It decreases in exponential way until zero. (see fig. 10) Due to the inhomogeneities of magnetic field, the magnetization vectors rotate at different speeds, and different directions. Due to these differences, their contributions are cancelled by each other, and fast decay of the signal occurs. This fast decay implies that the effective transverse relaxation time T2*, which depends on the field inhomogeneities, can be considerably shorter than T2.

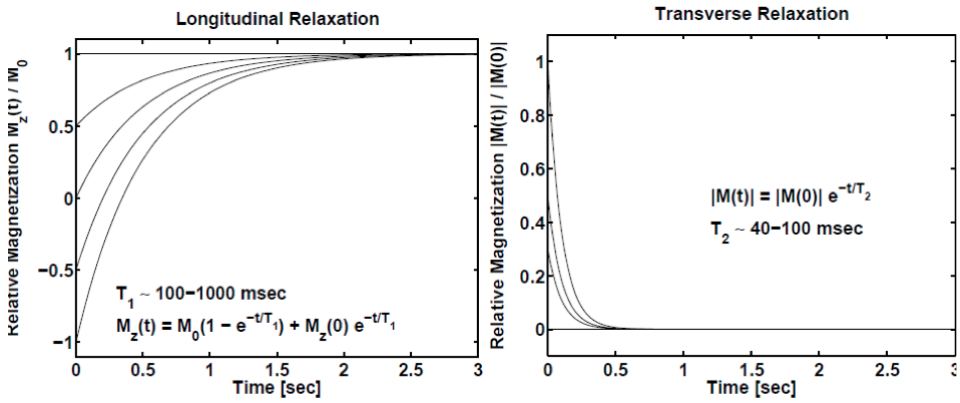

Figure 10 Trends of time constants T1 (left) and T2 (right) (Adapted from [5])

The values of T1 and T2 change between different tissues, because they depend on the constitutive molecules' properties. In this way, it is possible to distinguish different tissues of different apparatus but also, like in the case of the human brain, different segments of the same organ, that will be characterized by different intensities in the image.

The MRI technique allows obtaining three different kind of images: structural imaging, diffusion imaging and functional imaging. The first and second one give information about the anatomy of the brain, the latter gives information about the physiology of the brain.
They can be produced by using different exciting sequences on the tissue: gradient echo, echo planar imaging and spin echo sequence, In the next paragraphs, their main features are introduced.
The gradient echo sequence is used for functional imaging. The gradient is turned on in the x direction and the magnetic field increases linearly along it, protons at different positions precess with different frequencies, resulting in signal losses due to the dephasing of the spins. A reverse gradient is then applied, so that the magnetic field will increase in the negative x direction, and the signal builds up again. This process reduces the phase difference between spins, until the complete rephasing of the spins. When the spins are rephased they emit a signal of maximum amplitude. But the spin dephasing compensation only occurs for the gradients that are inverted, while all the other field inhomogeneities cause additional spin dephasing and thus reduce the T2* value. The time difference between the initial RF pulse and the center of the gradient echo is called echo time TE. Gradient echo images are T2* weighted and the choice of TE determines the T2* contrast.
Echo planar imaging is a special gradient echo sequence that has been implemented for reducing the acquisition time. After slice-selective excitation, a series of gradient echos are acquired by successive inversions of read gradient G_x. A short gradient pulse in y-direction, called blip, is switched on between successive acquisitions. The degree of phase encoding for a specific echo is given by the initial negative gradient in y-direction and the sum of the blips up to the echo acquisition time. A full image can be constructed from the data acquired. There is only one excitation pulse, so the technique is very fast. Usually, this sequence is used for fMRI acquisitions procedure[6].
In the case of spin echo sequences, two pulses are applied: the first one tilts the magnetization vector of 90°. After recording the first signal, a second pulse tilts the magnetization of 180° and a second signals is recorded. In detail, after the first pulse, all spins are aligned and they emit a strong signal. At this point, they start to rotate with different Larmor frequencies, and different speeds. When the second pulse is emitted the spins are rotated of 180° around the axis of initial alignment. In this stage, a spin overturning occurs, which means that previously slower spins become the quicker and viceversa. After a while the spins are realigned and a second strong signal (the spin echo)

is emitted. Using spin echoes sequence all field inhomogeneities are compensated, for this reason it is a T2-weighted method. [1][5][7]

1.2.2 MRI acquisition system

The MRI acquisition system is very expensive and voluminous medical equipment. It has to be placed in a specific room because the static magnetic field is characterized by the so-called magnetic fringe fields, which extend many meters from the magnet itself. Thus the filed attractive effect needs to be constrained in a well-defined environment to avoid accidents (for example projectile effect of metal objects). Furthermore the static magnetic field is always present even when the system is not in use.

The MR scanner is composed by three principal components (see fig. 11):

- Magnet;
- RF coils;
- Gradient coils.

Other components are: RF system generator, RF system detector, gradient pulse generator, hardware and software for images acquisition. For brain imaging, extra coils are used, they are defined head coil and are fixed around the head of the subject before starting the acquisition.

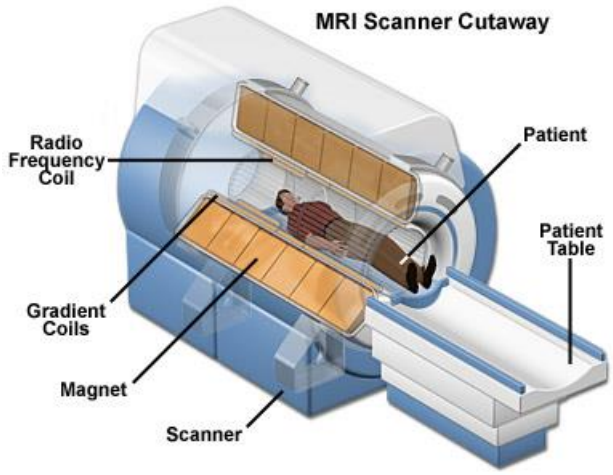

Figure 11 Scanner for MRI acquisition

During an MR investigation, the patient lies on a movable table that allows to move the subject inside and outside the scanner. The scanner is placed in a shielded room, because of the high strength of the static magnetic field and to avoid RF interferences with other devices outside the MR environment, while the computer for the acquisition is placed in the close control room.

Different MR scanners can be distinguished by the magnetic field strength. Nowadays, the static magnetic field has intensities from 1.5 T to 9 T. The most widespread MR acquisition systems have intensities of 1.5 T and 3 T.

Furthermore, there are different types of magnet: permanent magnet, resistive magnet and superconductive magnet. In the most recent scanners, superconductive magnets are installed. This type of magnet is constituted by superconductors materials which, at the temperature of a few Kelvin, can carry current without electrical resistance. In this way very stable magnetic field of high intensity can be generated by the current flow. In order to maintain a very low temperature for the magnet, the scanner has a liquid helium pump, called cryogen pump. A ventilation system is needed to control and maintain a good oxygen level in the room, because of the percentage of helium in the atmosphere could increase. During acquisition the gradient coils produce a very high level of noise (120 dB) so the use of headphones or earplugs is necessary for the subject in the scanner. [5]

1.2.3 Functional MRI

The fMRI technique provides functional images of the brain, which allow to understand which areas are active during a task (for example visual or auditory task) or during the resting state. [8]

fMRI is based on the fact that cerebral blood flow and neuronal activity are correlated; it detects changes in metabolic and hemodynamic signals that are indirect expression of the underlying local changes in neuronal activity.

The most commonly used fMRI contrast is the blood oxygenation level dependent (BOLD) signal [9], but it can be performed using also arterial spin labeling or injected contrast agents.

BOLD contrast relies on the use of hemoglobin as an endogenous contrast agent and this is possible because of the different magnetic properties of oxygenated and deoxygenated hemoglobin. The deoxygenated one is paramagnetic (paramagnetic materials are attracted by an external magnetic field and generate induced magnetic field in the same direction of

it), while the oxygenated hemoglobin and brain tissues are diamagnetic (diamagnetic materials are repelled by an external magnetic field and generate low induced magnetic field in the opposite direction of it). When neurons fire, blood releases oxygen to them at a greater rate than to inactive neurons. This is called hemodynamic response, and it causes a change of levels of oxy-hemoglobin and deoxy-hemoglobin. Thus, the magnetic field, inside the scanner, can be distorted (due to the high level of deoxy-hemoglobin) and this distortion can be detected in order to measure neuronal activity in a specific area. The distortion of magnetic field leads to a change of relaxation time constant T2* value, in the activated areas, and therefore to a difference of the signal intensity in collected images. [7] Several studies have reported that a monotonic increase in metabolic and hemodynamic responses occurs subsequent to increases in neuronal activity. But at the same time, also non-linear relationship have been found, it could depend on stimulus condition. [10,11,12]. The BOLD response appears with a certain delay, a few seconds, after the neurons activation. This is because changes in blood flow occur over a much slower timescale (hundreds of milliseconds to seconds) than changes in electrophysiological activity (milliseconds or tens of milliseconds). In the recent years, neuroscientists have been investigating the relation between the BOLD response and the underlying electrophysiological activity. For this reason, growing interest has been dedicated to the development of new methods for performing fMRI acquisitions in simultaneous with EEG recording which allow to better understand brain activations at different temporal scales (see next section 1.3). [1]

1. 3 EEG – fMRI technique

In the previous sections of this introductive chapter, general concepts about EEG and MRI technique have been discussed. In this section, the integration of the two techniques during simultaneous acquisitions will be described.

The combination of EEG and fMRI constitutes a powerful tool for the non-invasive investigation of brain functions and its dysfunction in presence of diseases. Using these two techniques simultaneously, it is possible to obtain information characterized by high temporal resolution (from EEG) and high spatial resolution (from fMRI). Indeed, the spatial resolution is about a few millimeters, while the temporal resolution is about a few milliseconds. [1,7]

Simultaneous EEG-fMRI allows to investigate functional connectivity of the brain, during resting state and during task-related activations. This technique was implemented for the first time in 1992 for localizing electrical sources of epileptic discharges. [13]

For integrating EEG and fMRI data, three different approaches can be adopted: 1) integration through prediction, 2) integration through constraints and 3) integration through fusion. [14]

The first approach involves the use of EEG data to form a model of the expected BOLD signal changes, by convolving the time-course of a particular component of the EEG signal with the hemodynamic response function to form a regressor. This regressor provides a prediction of the time-course of BOLD signal changes linked to the particular EEG component. Then, statistical analysis is performed in order to identify voxels in the image whose signal variation is significantly correlated with the regressor. In this way, a map identifying areas where BOLD signals are consistent with the variation of the chosen EEG components is obtained. The first studies used the power of EEG signal in the alpha-frequency band and tested for correlation with BOLD signal changes in the resting state, when alpha activity is most relevant [15]. Subsequent studies have evaluated correlations between BOLD signals and power in other frequencies bands, at rest and during task performance. [16,17]

With the second approach, integration through constraints, fMRI data are used to provide spatial constraints for localizing the sources of EEG signals. Several studies showed through separate analysis of data from the two modalities that hemodynamic activity and electrical responses were localized in the same brain areas. But this type of fusion should be performed with caution for several reasons: there may not be a corresponding BOLD response if low metabolic demand is generated by the neuronal activity responsible for a particular EEG signal; an EEG response may correlate to either a positive or negative BOLD signal making it difficult to know how to impose source constraints on the EEG. [18]

The third approach is the only one that does not perform a separate analysis of the EEG or fMRI data as first step, and it consists in the pure integration of the two signals. A proper data fusion analysis requires a common temporal forward model that links the underlying neuronal dynamics of interest to the measured hemodynamic and electrical response [14], but further work is needed before this approach can be more widely exploited.

1.3.1 EEG instrumentation in the MR environment

In order to perform simultaneous EEG-fMRI recordings, the EEG instrumentation needs to be MR compatible. Therefore some factors must be taken into account:

- the prevention from the introduction of ferrous materials into the magnetic environment;
- the limit of radiofrequency emissions to preserve image quality;
- the presence of static and time-varying magnetic fields;
- the EEG artefact associated to the magnetic fields.

Thus the electrodes are made by nonferromagnetic materials and the amplifier is shielded in a nonferromagnetic box.

The presence of magnetic fields can induce an electromotive force $V_{induced}$ in a conductive loop. Therefore the wires in the net must be checked and that the subject should not cross its arms or legs.

This $V_{induced}$ is proportional to the rate of change of magnetic flux cutting the loop $\frac{dB}{dt}$ and the loop area A. It can be calculated by the formula:

$$V_{induced} = A \times \frac{dB}{dt} \qquad (2)$$

The $V_{induced}$ can introduce artefacts in the signal, therefore minimize the area of any loop formed by electrode leads is important to reduce the artefact. To achieve it, electrode leads are joined in a single point on the head and the wires are twisted together from the subject's head to the amplifier input.

Another factor referred to the electrodes lead is the movement. Some proposed solutions are: weighing down the leads passing out of the scanner, electrodes secured by a tight bandage, head fixed by vacuum cushion.

The magnetic environment introduces two kinds of interferences that are very small in EEG recordings outside the scanner.

The first one is the pulse related interference, which is caused by cardiac-related movement of the electrodes or blood flow in the head. To remove this contribution, EEG instrumentation is supplied with additional electrodes for recording ECG signal. The ECG signal will be used to implement methods for removing this interference even if the completely removal of this interference is still a challenging issue (see chapter 3).

The second interference is related to the electromotive force induced in the electrode lead loops by the changing magnetic fields during the imaging acquisition. To decrease its contribution changes are required on the acquisition parameters, for example on the filtering, sampling rate and dynamic range.
Another important issue is patient safety. The presence of changing fields in fact can be dangerous for the following mechanisms:

- Eddy current heating;
- Current induced in loops formed between the electrodes leads;
- Current induced along electrode leads.

Moving through the static field, a current can be induced in an electrode lead loop, flowing between electrodes and hence in the patient, but this effect is very small in a magnetic field of 1.5 T. Thus at this magnitude, additional safety measures are not required whereas they should be take.
Gradient fields induce electromotive force in electrode loops, as described before, and this force is proportional to the rate of change of magnetic flux cutting the loop and the loop area. The dominant physiological effect is neuromuscular stimulation. [19]
The RF fields can induce eddy currents in the electrodes that are much greater than those induced in human tissues but the eddy currents may result in Joule heating of the electrode. Studies about this phenomenon have demonstrated that it is more significant with a static magnetic field of 4 T.
Thus any kind of loop in the wires has to be avoid in order to do not cause heating in the patient.
[1,6,20]

1.3.2 EEG-fMRI acquisition protocol

To perform an EEG-fMRI experiment, is necessary to define a protocol able to reduce interferences on EEG signals and to guarantee subjects safety.
The experimental protocol is divided in six steps:

1. Preparing the experimental setup
2. Preparing subject

3. Setting subject up inside the MR scanner
4. Recording signals and images
5. Debriefing the subject
6. Clearing up at the end of experiment

1. Preparing the experimental setup

Set up the EEG equipment in the control room; ensure the workspace for recording the data is set to the highest temporal resolution available and correct filter settings (data can be collected with a sampling rate of 1kHz and filtered with a 0.016-250 Hz band pass filter). Set up the MR scanner in the conventional way and turn on the synchronization of the scanner and EEG clocks. Check if the synchronization is successful. Set up the TR of MR sequences to a multiple of the EEG clock period (this is necessary for a good removal of imaging artefact, see chapter 3).

2. Preparing subject

Before starting to set up the EEG cap on the subject, it is important to explain him/her the aim of the experiment and what will happen. Ask the subject to fill out the forms, in which the MR scanning safety rules and constrains are presented and to sign them. In this way, the subject consents to participate to the experiment. At this point start the procedures for the placement of the EEG cap: measure the head-circumference and select the appropriate sized cap. Place the cap on the head starting at the front of the head and pulling backwards. Positioning the cap such that Cz electrode (the vertex reference) is sited half way between the nasion and inion and also centered left-right. The electrodes' impedance must be checked. The electrode (or electrodes) for the detection of ECG signal needs to be placed on the back or on the chest.

3. Setting subject up inside the MR scanner

Take the subject into the scanner room and ask him/her to lie on the scanner bed. The subject has to wear earplugs, headphones, because of high noise level caused by switching gradients. Arrangement of head coil over the subject's head. The EEG cables must leave the head coil along the shortest path possible. At this point, subject's head must be pad in order to minimize head movement. Attach the EEG cap to the amplifier, which is connected to the instrumentation by fiber optic cable, in the control room. There must not be wire loops in the EEG leads (as these can lead to RF heating and also cause larger EEG artifacts

to be induced) and that the cabling needs to be isolated from MR scanner vibrations as much as possible.

4. Recording inside the scanner

Switch off the helium pump during data acquisition. Before starting to acquire EEG data and scanning, the software for the EEG signals acquisition needs to be test if it is working well (for example asking to the subject to move the head, close and open eyes).

5. Debriefing the subject

When the acquisition is completed, take the subject out of the scanner and help him/her to take off the EEG cap.

6. Clearing up at the end of experiment

At the end of the acquisition, these steps are needed: check out of the participant, pack up the EEG equipment, cleaning the EEG cap (usually using water and disinfectant mixture). [7, 19, 21]

Chapter 2 – Imaging Artefact & Ballistocardiographic Artefact

Simultaneous recording of EEG signals and MR images is a powerful approach in the field of neuroscience. It allows obtaining information about brain functioning with high temporal resolution and high spatial resolution at the same time.

However, the combination of these two procedures increases the presence of artefacts in the EEG signal, thus obscuring the signal of interest. The artefacts are caused by the interactions between the subject, the EEG electrode assembly and the scanner's magnetic fields.

The main causes of EEG artefacts in the scanner are: 1) gross movements in the static field, 2) the ballistocardiogram (BCG) and blood flow effects in the static field associated with the subject's cardiac activity, 3) the changing fields applied during MRI images acquisition [22,23], 4) scanner vibration, 5) vibration due to the helium pump. [1]

The artefact associated to the scanner and helium pump vibrations can be attenuated by some precautions (see section 1.3.2). On the other hand artefact sources related to the cardiac activity and to the gradients switching need to be post-processed and big efforts have been done to implement methods for their removal. This chapter focuses on the imaging artefact and the BCG artefact (see fig. 12). Their origins and their removing methods will be henceforth presented.

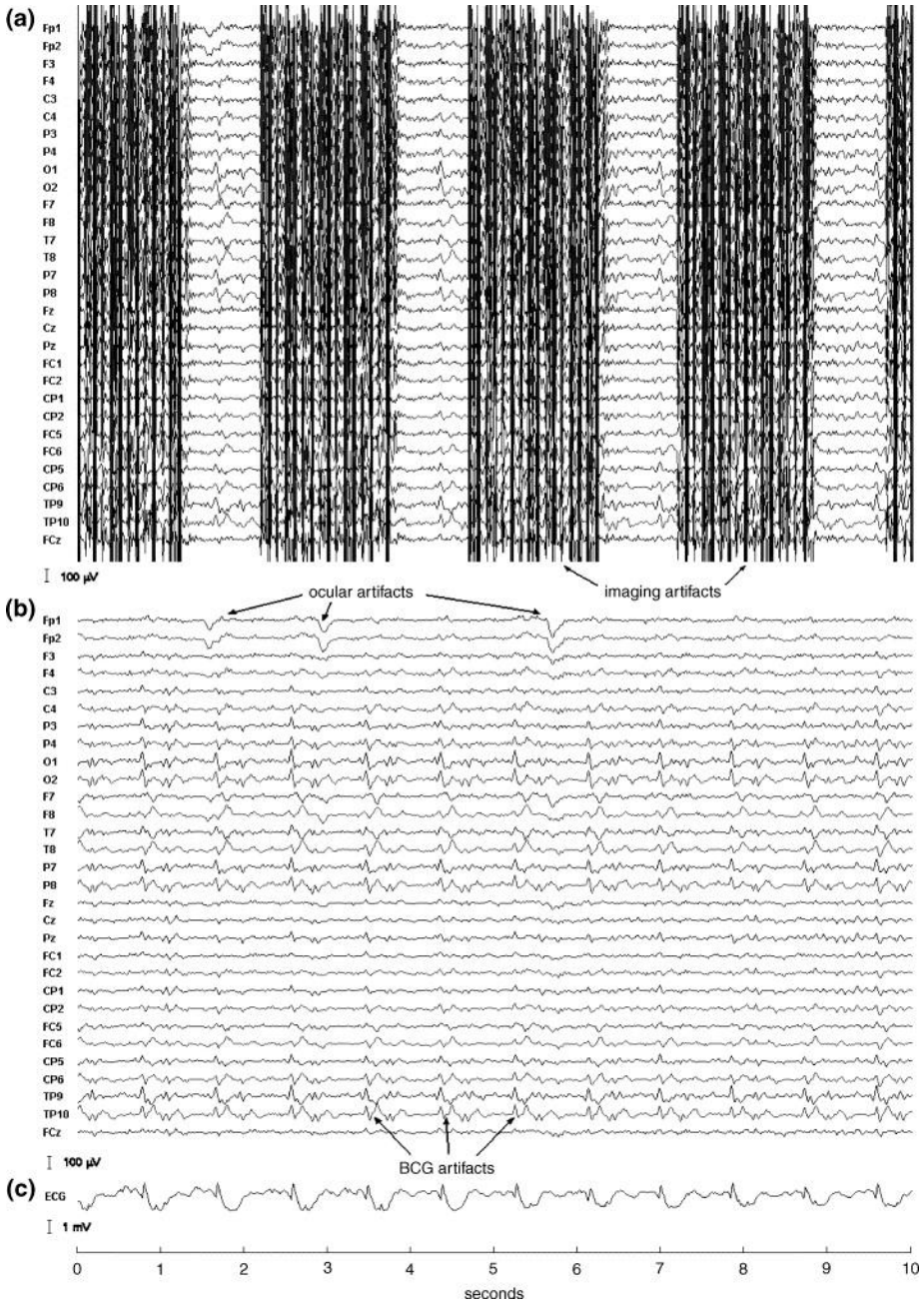

Figure 12 (a) EEG signals corrupted by imaging artefact. (b) EEG signals after imaging artefact removal but corrupted by ballistocardiographic artefact. (c) ECG trace (Adapted from [34])

2.1 Imaging Artefact

Many studies were performed in the past twenty years for characterizing and removing the imaging artifact. In the next paragraphs, the main findings about this artifact will be introduced.

Imaging artefact is induced by magnetic fields applied during images acquisition. Two different fields are applied: RF and gradients (G_x, G_y, G_z)(see chapter 1, section 1.2.1).

The artefact is characterized by: 1) consistent waveforms, each peak component corresponded precisely to an RF and gradient pulses; 2) the artefact associated to the gradient pulse has its amplitude in the order of 10^3-10^4 μV, while the amplitude of the artefact generated by the RF pulse can be up to 10^2 μV; 3) an artefact component caused by one gradient pulse consisted of a pair of peaks, one of which deflected positively or negatively and the other inversely, thus the artefact from one gradient pulse has the differential waveform of the corresponding gradient pulse; 4) artefact induced by RF has a much higher frequency then EEG. While the gradient artefact is characterized by components in the EEG frequency range. (see fig. 13) [23]

The amplitude of induced gradient artefact is given by Faraday's law (chapter 1).

Imaging artefact depends on scanning process, which is a preprogrammed process, thus this artefact has a strong deterministic component. The relative polarity and amplitude of the artefact varies across EEG channels, but the timing of the rising and falling edges are the same across channels. This repeatability allows to efficiently remove the imaging artefact, by subtracting an artefact template from the EEG signals.

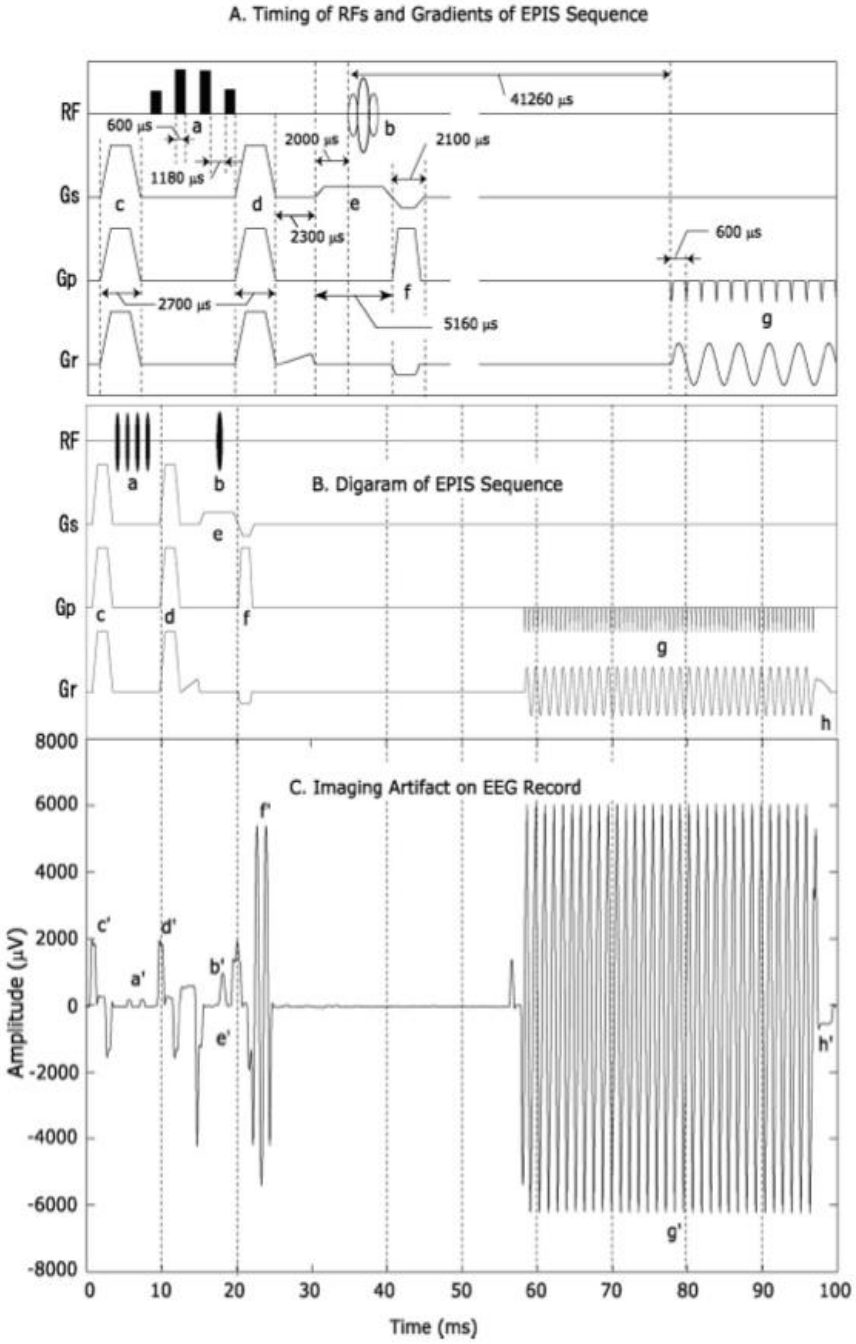

Figure 13 (A) Timings of RF emission and gradients pulses in an fMRI sequence. *RF*, radiofrequency wave; *Gs*, slice selection gradient; *Gp*, phase encoding gradient; *Gr*, readout gradient. *a*, Fat suppression pulses (1-3-3-1 pulses); *b*, slice selection RF; *c*, *d, h,* spoilers; *e*, slice selection gradient; *f*, dephasing and rephasing gradient; *g*, readout gradient. (B) Schematic diagram of whole EPI (echo planar imaging) sequence. (C) Imaging artefact waveform for one slice scan on a dummy EEG record with a phantom using the EPI sequence. The artefact corresponding to each gradient component described above in (A) can be identified, and it is denoted by the same alphabet as the one denoting the original gradient but with a prime. [23]

2.1.1 Method for removing the Imaging Artefact

The most used method for imaging artefact removal is based on the averaged artefact subtraction (AAS) and was proposed by Allen et al in 2000 [24]. The deterministic characteristics of the artefact allow constructing channel specific artefact templates, so this approach assumes that the shape of the gradient artefact does not change rapidly and that is not correlated with the physiological signal.

The artefact template is calculated channel by channel by averaging EEG epochs. The number of epochs is related to the TR of the sequence used for the acquisition in the scanner. Recording a marker in correspondence to each image acquisition occurrence is needed to identify the epochs.

Thus, the EEG signals are divided into epochs, each epoch containing an MRI volume or scan acquisition period. The epochs are then interpolated (for example by a sinc function with a factor of 10-15 [24]) and then aligned by maximizing the cross-correlation to a reference period. The epochs are averaged in order to obtain the template, which is subtracted from each epoch. In figure 14 the results are illustrated.

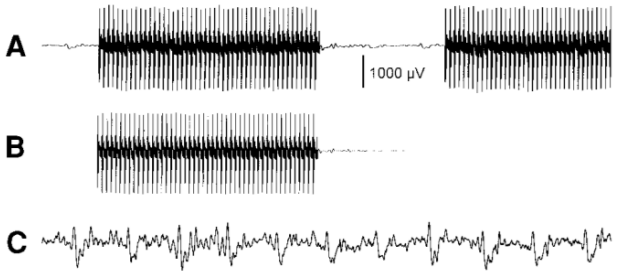

Figure 14 (A) EEG signals recorded in the scanner. (B) Averaged imaging artefact. (C) the result of subtracting the averaged imaging artefact in B from the EEG in A. (adapted from [24])

The most of the methods that have been proposed by researchers for correcting the imaging artifacts are based conceptually on the AAS. The several proposed algorithms differ with respect to the number and selection of averaging epochs and their weighting. [1]

Although subtraction of averaged artefact removes a large portion of the imaging artefact, residual artefact could be sometimes still present. There are two main causes for this: 1) jitter between the EEG sampling and scanner time frames; 2) differences between individual epochs and the average artefact, due to small subject movements. Allen et al.

[24], in order to attenuate the residual artefact, applied an adaptive noise cancellation (ANC) filtering procedure.

However, to attenuate residual artefacts, it is also important the instrumentation for recording the EEG signals, because without a suitable acquisition, the artefact features can be lost or changed and this could cause a bad removal (see chapter 1, section 1.3.2). [24][25]

2.2 Ballistocardiographic Artefact

The Ballistocardiographic (BCG) artefact is related to the cardiac activity of the subject. Since it arises from slight electrode movements in the static magnetic field, it can be observed in absence of scanning for the images acquisition [22]. The movement could be due to the local effect of pulsatile movements of scalp vessels on adjacent electrodes (ballistic effects). This effect is called pulse-driven expansion. The pulsatile movement can cause the expansion of the scalp, especially in areas on the major vessels (e.g. the temporal artery). [26]

Another contribution to the BCG is induced by cardiac pulse-driven rotation of the head in the strong static magnetic field of the MR scanner. This rotation is driven by changes in the momentum of blood as it is pumped by the heart and shunted into the head arteries. [27]

Motion of blood in arteries and veins can induce Hall effect and, thus, give another contribution to the BCG artefact. The ions in a conducting fluid, such as blood, experience a force when the fluid flows in an applied magnetic field. The force is given by

$$F = q\boldsymbol{v}\times\boldsymbol{B} \qquad (3)$$

where q is the charge of the ion, v is the flow velocity, and B is the applied magnetic field. Thus, any ions with a component of motion orthogonal to the magnetic field will experience a force whose direction is orthogonal to the plane containing both the velocity and magnetic field vectors. Positively and negatively charged particles move in opposite directions, accumulating on the vessel wall until equilibrium is established. The charge distribution on the vessel also produces an external field that causes current flow in the surrounding conducting tissue. A scalar potential is consequently produced at the surface of the body and detected, for example, by surface electrodes as used in EEG measurements. The resulting potential is proportional to the blood velocity and it is expected to show a periodic variation through the cardiac cycle. [27,28]

Although the artefact is mainly caused by these three effects, it is still not clear which is the degree of contribution from each of them even if, probably, the major contribution comes from the pulse-driven rotation [27,29]. These causes were identified using computational models, in parallel with acquisition in vivo, and recordings of EEG signals in vivo adopting different strategies to diminish the described mechanisms and obtaining signals with a lower contribution of BCG artefact [27, 28]. For example Mullinger et. al [27] used a bite-bar and vacuum cushion to restrain the head and observed greatly attenuating contribution of cardiac-driven head rotation.

It is a matter of fact that this artefact is related to the cardiac activity, thus to studying it, an electrocardiographic (ECG) signal is usually recorded during the EEG-fMRI acquisition. One or two electrodes of the cap are employed to measure the ECG signal and they are attached either on the back or in correspondence of the left side of the heart of the subject [21]. In figure 15, some EEG recordings affected by the BCG artifact are illustrated.

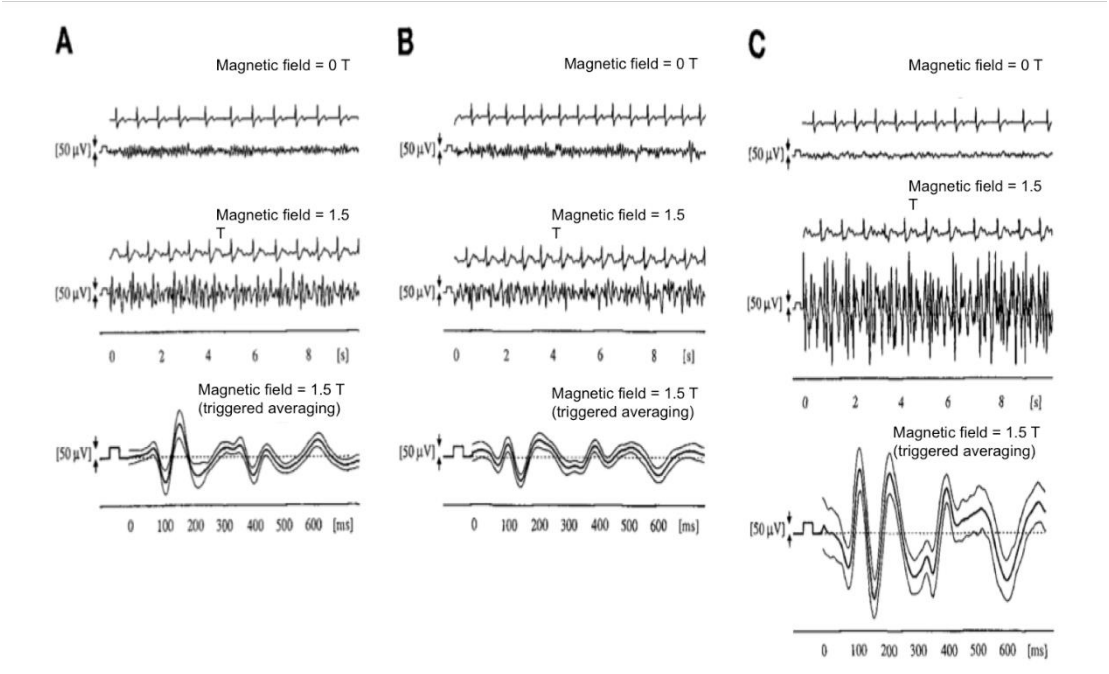

Figure 15 Simultaneous recording of EEG and ECG in one subject, at (A) occipital (Pz-Oz), (B) parietal (P3-O1), and (C) frontal (F3-Fp1) electrode positions. Upmost rows show ECG and EEG recording outside the magnet. The two traces in the middle show the signals in the same volunteer inside the magnet at identical electrode positions. The lowest trace presents the EEG recording, averaged by ECG triggering (curves are mean ± 1 SD). (Adapted from [22])

Müri et al. [22] observed that there was a large difference between EEG signals recorded outside and inside the scanner. For signals detected in the static magnetic field, after a

certain delay from the QRS complex in the ECG, specifically after the R wave, a high contribution added up to the EEG signal and the amplitude was much larger than the amplitude outside the scanner. Furthermore, the amplitude changed across the scalp. For example, signals recorded from the frontal electrodes showed a large magnitude compared to the signals recorded in the occipital and parietal electrodes. In the study, the authors supposed that the pulse-related head movement was greater at the front of the head compared to the rear, which rests on the scanner table and under the head coil. The adherence of the electrodes with the scanner table decreases the electrodes movement and therefore the BCG artefact contribution, as shown in successive study. [28]

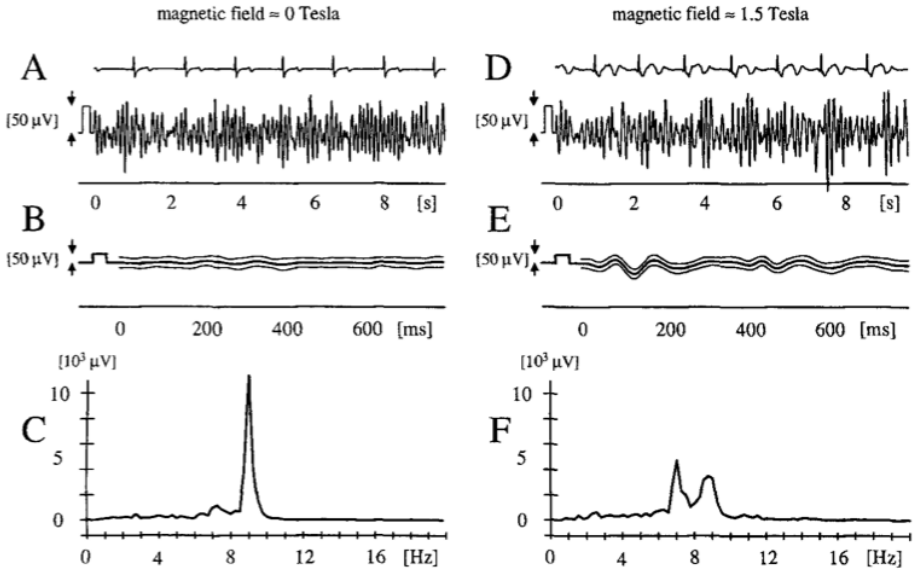

Figure 16 EEG signal at the occipital (Pz-Oz) electrode position, (A)-(C) outside the MR scanner, (D)-(F) inside the scanner. Rows (A) and (D) show simultaneous ECG and EEG recordings. The curves in (B) and (E) represent mean ± 1 SD of the EEG recording, averaged by ECG triggering. Rows (C) and (F) display the power spectra obtained by fast Fourier transformation of (A) and (D), respectively. The additional peak at 7 Hz in the Fourier transformed signal recorded in the magnet indicates additional components**.** (Adapted from [22])

In the same study [22], a variation in the frequencies range was observed. In particular, additional peaks in the power spectra were found confirming the presence of additional components in the EEG signals (see fig. 16).

In later studies, the BCG artefact was deeper investigated, observing that it could be composed by several peaks, with different delays from the R peak from the ECG and with different amplitudes. It is characterized by strong variability in terms of: amplitude of BCG

peaks, morphology of the artefact and time occurrences of the BCG peaks. The delay between the R peaks and the first strong peak of the artefact in the EEG traces has been estimated of approximately 200 ms. [30]

It has been supposed that the first peak could be associated to the pulse-driven expansion movements while the second one to the pulse-driven rotation (see fig. 17). [29]

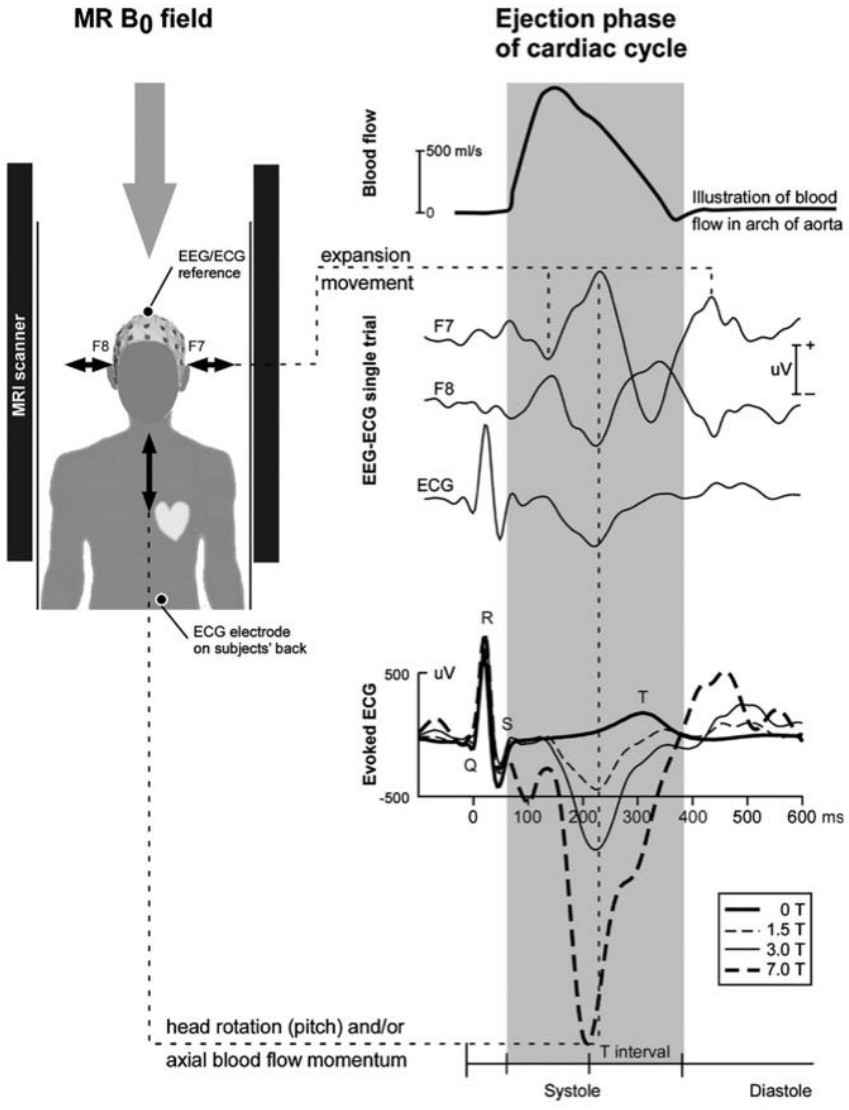

Figure 17 A model illustrating two contributions to the BCG. The left-hand side of the figure indicates a participant in supine position in a MRI scanner. The polarity of the BCG artefact depends on the direction of the static magnetic field, which is different for MRI scanners from different manufacturers. The upper right- hand side of the figure illustrates the time course of blood flow over the cardiac cycle. Shown below is a single EEG trial at two left and right hemisphere electrodes (F7, F8), and the corresponding ECG trace. Note the systematic polarity reversal over time during the ejection phase of the cardiac cycle, indicated by a grey background. The lower right-hand part of the figure shows the evoked ECG traces. (Adapted from [29])

The amplitude of the BCG artefact can be comparable to or higher than the one the of brain signal. The BCG artifact amplitude can be in the range of 50-200 μV, or even more, and the frequencies are overlapping with the frequency range of the brain activity, as showed in figure 18. However, it is noteworthy that the amplitude of the artefact strongly depends on the magnitude of the static magnetic field. Debener et al. [29] recorded EEG signals in static magnetic field of 1.5 T, 3 T and 7 T. They found that the amplitude of the BCG artefact scaled approximately linearly with the static magnetic field strength (see figure 18). Furthermore, they also found that the spatial variability increased at higher field strength, as a consequence of the increase in the absolute magnitude of the BCG. In other words, the topographical variability of this artefact was less pronounced at 1.5 T compared with 3 and 7 T. This information is relevant for an appropriate removal of the artefact.

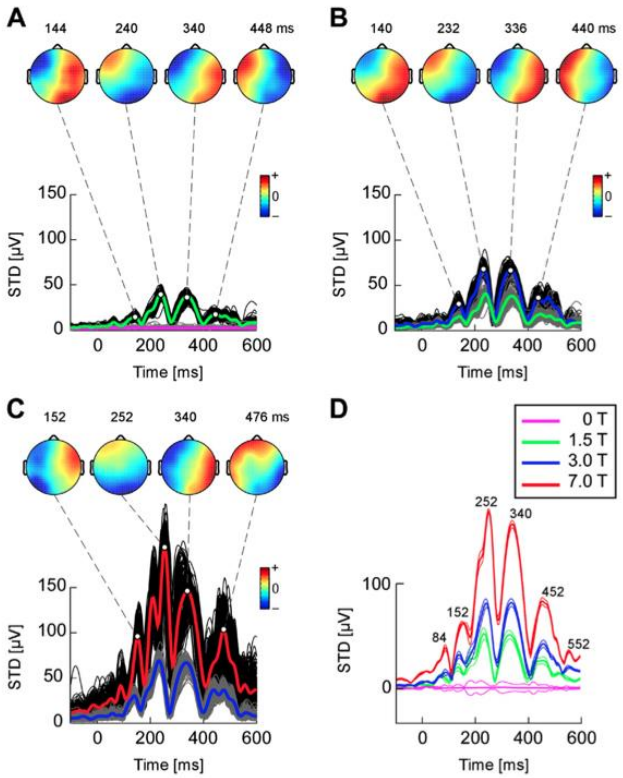

Figure 18. (A) Comparison of outside the scanner (grey) and inside 1.5 T MRI scanner single-trial GFP traces, expressed as standard deviation (STD) over time, with 0 ms denoting the onset of the ECG R wave. Colour-code of mean traces is shown in D. (B) Same comparison as in A, for 1.5 T (grey) and 3 T (black) data. (C) Same comparison as in B, for 3 T (grey) and 7 T (black). (D) Group mean GFP (± standard error of the mean), overlaid for recordings outside the scanner (0 T) and at 1.5 T, 3 T and 7 T. Peak latencies are indicated for the 7 T mean GFP data. (Adapted from [29])

Furthermore, the static magnetic field has an influence on the polarity of the BCG peaks. In particular, the polarity is opposite between left and right hemispheres and it would reversed in a field with opposite direction. (see fig. 18) [29]. If the static magnetic field has a head to foot direction, the highest peak of BCG are positive on electrodes located in the left hemisphere and negative in the ones located in the right side of the head [31].

Due to the very high variability of the BCG artefact and its complex contribution to the EEG signals, a detailed characterization is required. An appropriate evaluation of this artifact features can provide an important basis for developing methods for properly removing it from the EEG recordings and recovering the information about brain activity from the cleaned EEG signals.

2.2.1 Methods for removing the BCG Artefact

So far several methods have been proposed to reduce the BCG artefact and to improve the EEG signals quality.
The methods, which will be presented in detail in the following paragraphs, are based on different procedures:

- Average Artefact Subtraction (AAS);
- Principal Component Analysis (PCA);
- Independent Component Analysis (ICA).

Method based on Average Artefact Subtraction

The first method was implemented by Allen et al. in 1998 [30]. They introduced the AAS algorithm. This method relies on the hypothesis that the artefact is relatively stable across a number of successive heartbeats. The algorithm's aim is to create a template of the artifact to be subtracted from the EEG signals. The idea is similar to the one implemented for removing the imaging artifact, with the difference that the epoching of the data is performed by using as triggers the information from the ECG signal.
The first step of the algorithm consists in the identification of the ECG peaks, i.e. the R peaks of the QRS complex. Then, a template is calculated by averaging the epochs of the R peaks triggered EEG signals. Finally, the template, specific for each channel, is subtracted epoch by epoch.
More in detail, the EEG signal is epoched channel by channel, and each epoch is defined as a time window centered on the R peaks instant and having as length the mean R-R interval. This time interval is necessary because the BCG peak normally occurs a short time after the QRS complex (see previous section), this delay was assumed equal to 210 ms. The

epochs are averaged (removing epoch that contains other artifacts), obtaining the artefact template that is subtracted from EEG signal (see fig. 19). The procedure can be implemented also in real time.

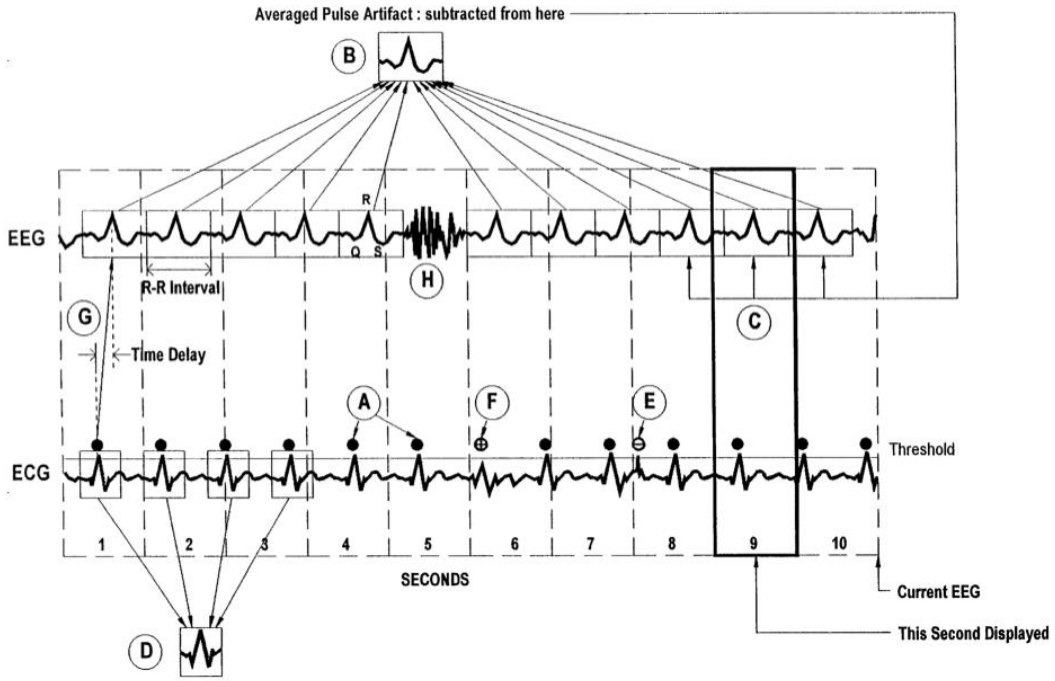

Figure 19 This shows a schematic view of the BCG subtraction method. (A) An ECG peak corresponding to a QRS complex is detected. (B) BCG waveforms in the EEG channels, time-locked to the ECG peaks are averaged. (C) The averaged BCG signal for each channel is subtracted from the EEG signals at times corresponding to the ECG peaks. (D) To confirm that an ECG peak detection corresponds to a QRS complex, an averaged QRS waveform is calculated from the first four ECG peak detections with temporal characteristics which indicate a high probability of being QRS complexes. This is then cross-correlated with the ECG waveform at each peak detection. (E) ECG peaks corresponding to noise in the ECG signal are rejected due to a low value of cross-correlation with the averaged QRS waveform calculated in D. (F) QRS complexes which are not detected by threshold crossing are added. (G) The sections of EEG (duration ± half the mean R–R interval) occurring a short time interval after the ECG peaks are averaged. A time interval is necessary as the peak of the BCG in an EEG channel normally occurs a short time after the QRS complex. (H) If the section of EEG time locked to an ECG peak contains other artifacts, the section is excluded from the average BCG waveform. (Adapted from [30])

The quality of the template should increase with the number of epochs used, but averaging more epochs could reduce the sensitivity of the template to capture temporal fluctuations of the artefact. Furthermore, this method cannot take into account of the large variability of the BCG artefact, as previously described, thus it leads to non-negligible residual artefact after the subtraction.

Also, the choice of the template length may be problematic due to the variations in the R-R interval, as the subject's heart rate is variable. Consequently, mismatch between template

window length and artefact duration would lead to residual artefacts. So different strategies have been proposed for a better generation of the template, for example by using weighted averages or median instead of the mean values. [30]

Methods based on Principal Component Analysis

Another algorithm that improves the quality of EEG signals, removing the BCG artefact, is based on Principal Component Analysis (PCA). The PCA is a statistical procedure that uses an orthogonal transformation to convert a set of observations of possibly correlated variables into a set of values of linearly uncorrelated variables called principal components. The number of principal components is less than or equal to the number of original variables. This transformation is defined in such a way that the first principal component has the largest possible variance (the highest content of information). The other components are orthogonal to the first one and between them and the associated variance has decreasing value from the first to the last component.

The method is called Optimal Basis Set (OBS) [25], and it differentiates from the AAS for the different artefact template generation. The assumption is that over a sufficient period of EEG recording from any single EEG channel, the different BCG artefact occurrences in that channel are all sampled from a constant pool of possible shapes, amplitude and scales. Furthermore, each occurrence of a BCG artefact, in any given EEG channel, is independent of any previous occurrence. The principal components of all occurrences can then describe most of the variations of the BCG artefact in that channel. The PCA is applied on a matrix of BCG artefact occurrences, channel by channel. This method takes into account a constant delay between the R peaks in ECG signal and BCG peaks in EEG signal of about 210 ms, as proposed by Allen et al. [30].

In the current paragraph the main steps of this method are summarized. First of all, after the detection of the R-peaks from the ECG, the R peaks are shifted forward in time by 210 ms in order to identify the BCG occurrences in the current EEG channel. Then, in the second step, for each channel, all BCG artefacts occurrences are aligned in a matrix and PCA is performed. The optimal basis set is made up of the first three or four principal components [32]. The OBS is then fitted to, and subtracted from, each BCG artefact occurrence. The process is repeated for each channel.

Thus this approach, unlike AAS, can take into account for greater temporal variation in the artefact shape, leading to lower quantity of residual artefact than AAS procedure, as shown in figure 20. [25]

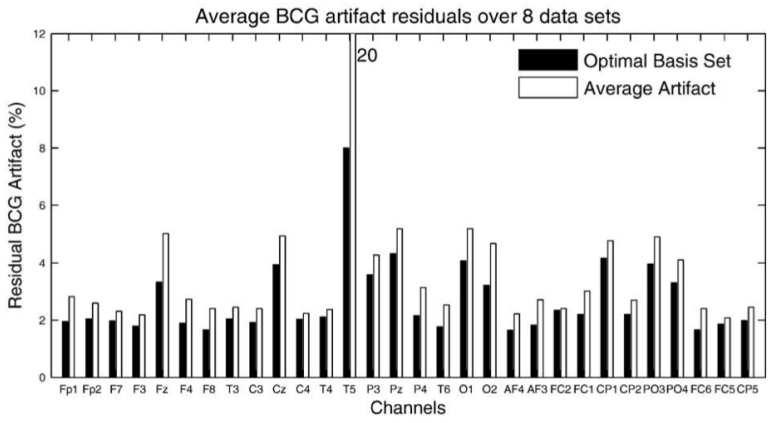

Figure 20 Plot illustrating the amount of BCG artifact residuals left by the AAS and OBS methods. The height of each bar is the percentage of the original BCG artifact power for that channel that still remained as residuals after cleanup. The shown results are the average over 8 data sets. On average using OBS left 2.7% residuals while AAS left behind 4.0% of the original BCG artifact power. (Adapted from [25])

Methods based on Independent Component Analysis

The Independent Component Analysis (ICA) is a signal processing technique that can be used to recover independent sources from a set of simultaneously recorded signals that result from linear mixing of the source signals. Accordingly, the methods based on the ICA hypothesize that the BCG artefact contribution is physiologically independent from ongoing EEG activity, since the generator of the artefactual activity comes from the cardiac pulsation and not from neurophysiological source.

Unlike the previous described methods, ICA technique does not make assumptions about the shape of the source signal, but the assumption is that the sources are supposed to be stationary in time and space.

When applying the ICA on an EEG dataset, the output is composed by a number of components, equal to the number of the EEG signals given as input. Since, these components are independent, some of them are associated to artefactual activity, while others to brain signal. It can be difficult to visually identify and select the components that represent the BCG artefact because their number and shape are not precisely defined. The

methods proposed in literature differ for the technique used to detect the artefact components among all the components in output and for the ICA implementation.

For example, Srivastava and colleagues [33] identify the BCG artefact components manually (considering temporal location, rate and duration of peaks in the component), but also correlating the components corresponding to the BCG artefact with either a simultaneously recorded ECG channel, or an estimate of the BCG artefact obtained by averaging the epochs of all the EEG channels.

In the same way Mantini and colleagues [34] used a manual approach based on visual inspection of the time course of each signal, together with the corresponding scalp map and power spectrum, and an automated approach based on the use of a reference signal, such as ECG. The occurrence of a large correlation value between the single independent component and the reference indicates that the source had to be considered as an artefact (in their study the ICs with a correlation value larger than 0.20 were classified as BCG components).

After the recognition of the ICs of interest, they are subtracted from the recordings with appropriate weights for each channel.

In general three to six BCG components can be expected after ICA processing (see fig. 21). Furthermore, using the ICA approach is possible to remove the residual imaging artifact, previously removed by AAS, and also other kind of artifact, such as the ocular artefact. [34]

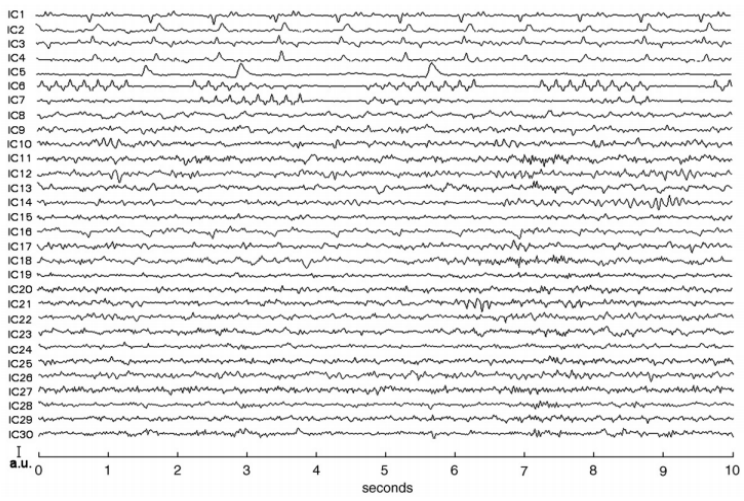

Figure 21 Sample segments of the 30 ICs separated with FastICA using the traces presented in fig. 13. The ICs 1, 2, 3 and 4 are BCG artifact components; the IC 5 is an ocular artifact component; the ICs 6 and 7 are components that can be ascribed to the imaging artifact residual. The amplitudes are arbitrary because the components are normalized. (Adapted from [34])

The ICA based methods have showed higher performance than AAS based method for the removal of BCG artefact.

In figure 22 the corrupted EEG data are illustrated, whereas in figure 23 the cleaned EEG data are illustrated.

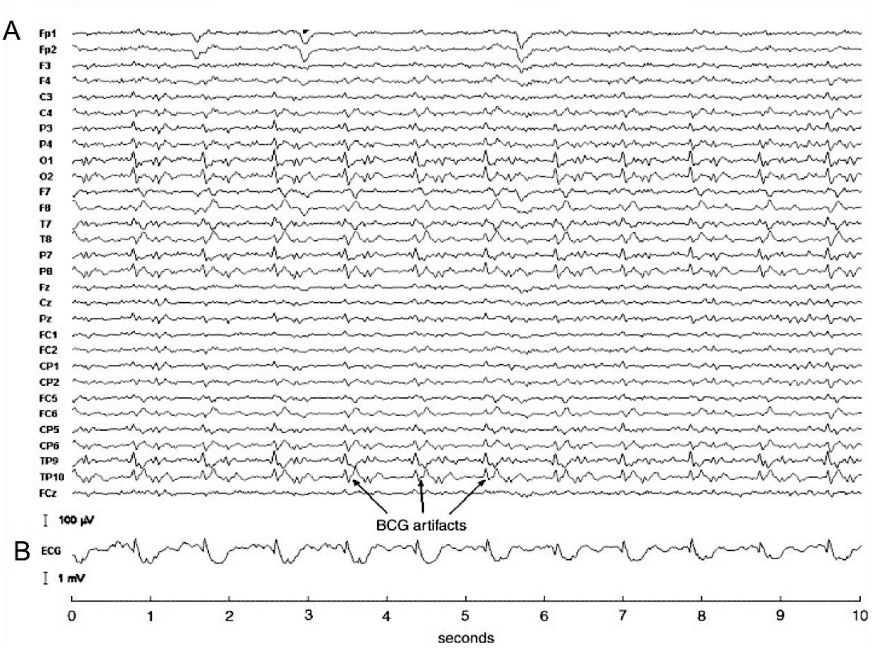

Figure 22 A. EEG data corrupted by BCG artefact, the effect is most visible on the temporal recordings. B. ECG trace, (Adapted from [34])

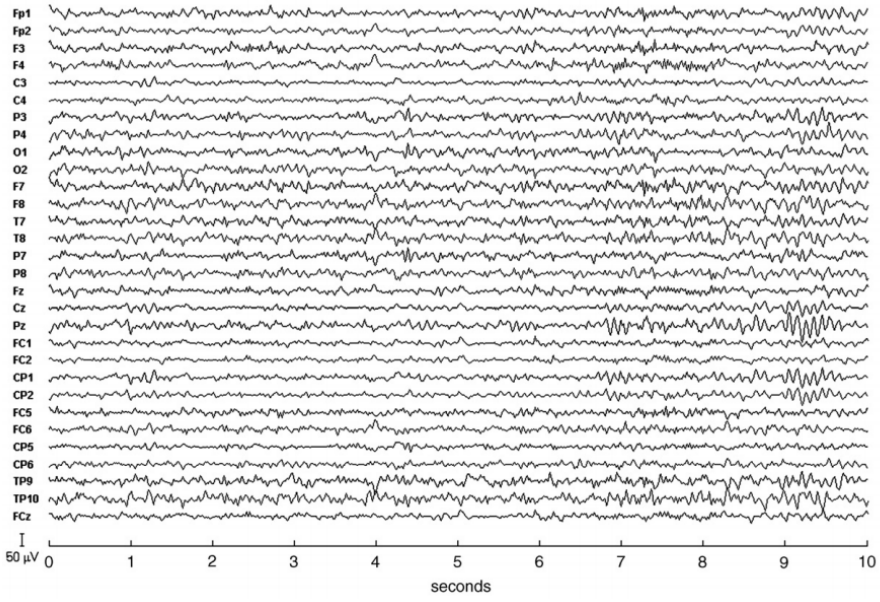

Figure 23 Artifact-free EEG data reconstructed using ICA with the traces in fig. 22.(Adapted from [34])

2.3 Thesis's Aim

In the previous sections several methods for removing the imaging and BCG artefacts have been described. It is important to emphasize that, nowadays, well-performing methods for the removing of imaging artefact have been implemented, because of stationary properties of this artefact. Whereas, implementing methods for a total removal of BCG artefact is still a difficult goal to achieve, this is due to the large variability of the artefact.

The AAS method is based on the subtraction of an average artefact template. Making this template it does not take into account of the variability between the BCG occurrances. Thus it can induce to large artefact residual. Furthermore a constant delay from the R peak in ECG is used to identify the BCG events. [30]

The OBS method performs the PCA on EEG signals extracting the principal components with the highest associated variance. These components describe different features of the BCG artefact and they are used to make an artefact template. Thus the OBS method, unlike the AAS method, takes into account the artefact variability. On the other hand, two factors can cause artefact residual: 1) the number of principal component used for making the template is not established and 2) it uses a constant time delay between the R peaks in the ECG and the occurrence of BCG peaks. [25]

The methods based on ICA do not make assumption on the artefact shape and this is a very positive aspect. Performing ICA on the EEG signals it is possible to obtain independent component describing just the contribution of BCG artefact, which can be subtracted from the EEG signal.

Three aspects negatively affect this approach. The first one is that these methods have different performance if the EEG signals are acquired in different magnetic field strengths. It has been found that, they work well on signals recorded in 1.5 T scanner (as demonstrated by Mantini et al. [34] and Srivastava et al. [33]) but not on signals recorded in higher magnetic field strength [29]. Maybe this is due to the larger variability of BCG artefact (see chapter 2) and a major distortion of ECG signal, so the correlations between the ECG channel and ICs can be expected to be rather low and unspecific, because the ECG channel contains prominent features that are virtually absent in the EEG and vice versa.

The second negative aspect is that most ICA algorithms assume stationary of the sources, since the BCG artefact shows a considerable variability between occurrences, satisfying this assumption can be problematic [32]. A proposed solution is to apply OBS prior to ICA removing the major part of the artefact with OBS and its residuals with ICA. [35]

The third negative aspect is that the number of independent components associated to the BCG artefact is not established.

Thus the aim of this thesis is to show concretely these problems analyzing the EEG data recorded and to find additional features of the BCG artefact. In the next chapters the methods used for the analysis and the results obtained will be described.

Chapter 3 – Materials & Methods

3.1 EEG-fMRI acquistion

Six right-handed healthy subjects (age 26.5±6.3 years, 4 males and 2 females) participated in the experiment. All participants reported normal or corrected-to-normal vision, and had no psychiatric or neurological history. Before undergoing the examination, they gave their written informed consent to the experimental procedures, which were approved by the local Institutional Ethics Committee of UZ Leuven.

Simultaneous EEG–fMRI resting-state recordings were performed for 10 minutes for each subject in a 3T Philips Achieva MR scanner (Philips Medical Systems, Best, the Netherlands)) using a T_2^*-weighted SENSE sequence. The scanning parameters were TR = 2000 ms, TE = 30 ms, 36 slices, 80 × 80 matrix, voxel size 2.75 × 2.75 × 3.75 mm^3, flip angle = 90 degrees.

EEG signals were recorded by the MR-compatible 256-channel HydroCel Geodesic Sensor Net (GSN) (EGI, Eugene, Oregon, USA), that includes a large number of Ag/AgCl electrodes on lower temporal areas and cheeks. Each electrode contains a small sponge soaked with saline solution that make contact with the patient's scalp and keep the electrodes impedance low (<50 kΩ) across the full recording. An elastic bandage was also placed above the EEG net to maintain the contact of electrodes on the scalp. During simultaneous EEG–fMRI recordings we also acquired the electrocardiogram (ECG) signal with two MR-compatible electrodes positioned on the chest, in correspondence to the apical part and to left side of the heart. The EEG and ECG cables passed through the front end of the bore to the MR-compatible amplifier positioned on the left side of the participant. The EEG amplifier itself is contained in a field isolation containment system (FICS), and MRI clock signals are synchronized with EEG data collection for subsequent MR artefact characterization and removal. EEG recordings are acquired at 1 kHz sampling frequency using the vertex (Cz) electrode as physical reference.

3.2 EEG Data processing

All the EEG processing procedures described in the next sections have been performed with functions implemented in MATLAB (MathWorks, Natick, US) and in the EEGLab toolbox [36].
In the following sections the methods applied for the signals processing and the characterization of BCG artefact will be described.
The executed steps are here summarized in the following figure:

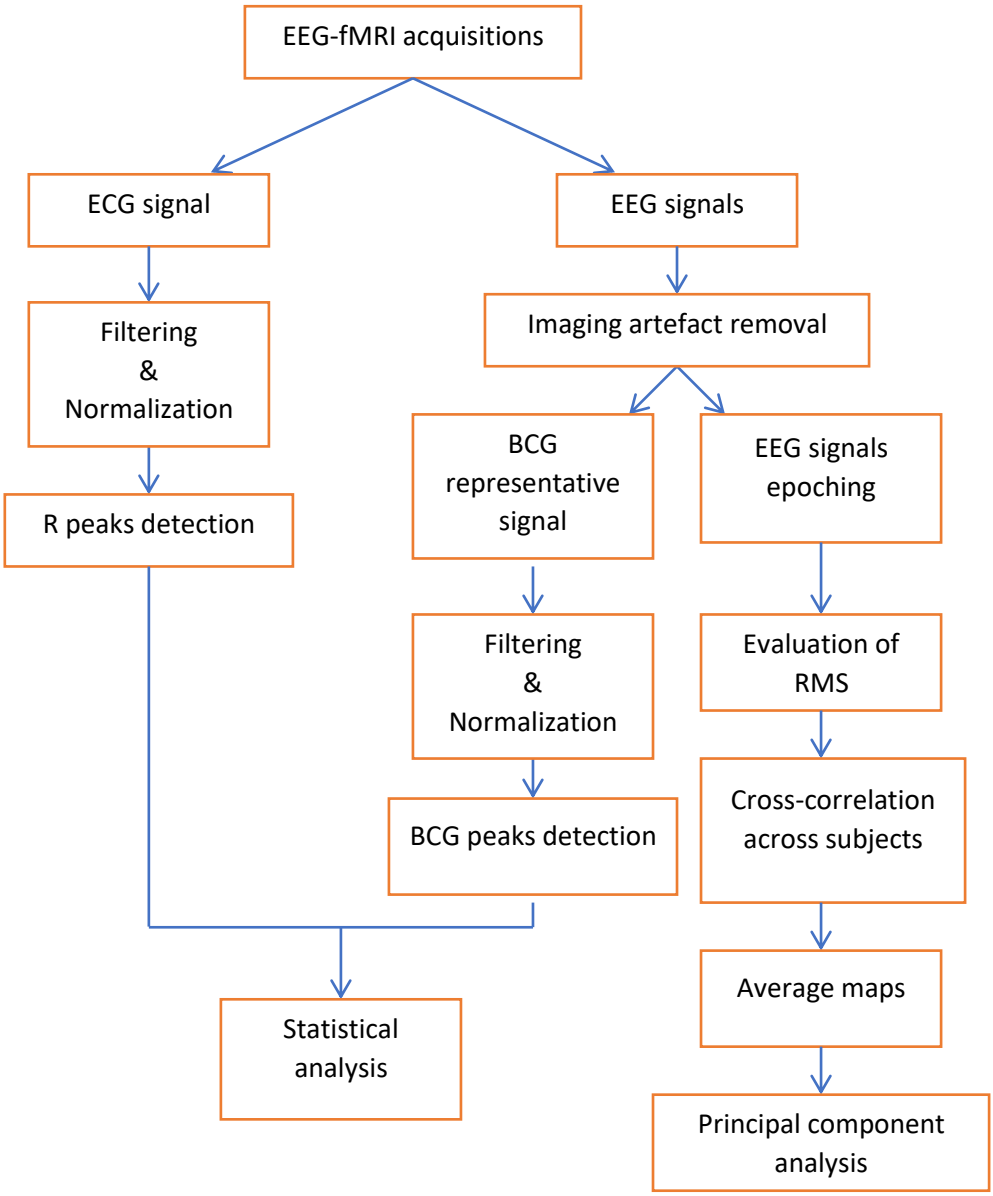

Figura 24 Flowchart describing the data processing steps

First of all, we need to remove the imaging artefact from the EEG signals collected in the MR environment. Thus the dataset is corrupted by only BCG artefact. In order to study the artefact and to have a time reference for its occurrences, we will create a signal representing the BCG artefact across channels. The detection of R peaks in ECG signal and BCG peaks will be performed. Another important procedure that will be performed is the epoching of the signals. The epoching of a signal consists in cutting it in correspondence of specific instants along the recording. The instants are defined by triggers (for example the ECG peaks). Thus what we obtain are several time windows of the signal, which are called epochs or trials. By averaging all the trials, the average information focused on a particular event (in this case the BCG artefact) can be obtained.
The average signals will be used for a further investigation about the activity of the BCG artefact across the scalp and its contributions. Thus an analysis across subjects will be performed and the principal component analysis will be used to better understand the contributions to the artefact.

3.2.1 Removal of Imaging Artefact

The first step of the EEG data preprocessing pipeline is the removal of the imaging artefact. This procedure is performed by using the fMRI artefact slice template removal (FASTR) method proposed by Niazy et al. [25] and implemented in EEGLab. The method consists in: a first stage in which the artefact template subtraction (AAS) method is performed and a second stage in which the artefact residuals are estimated using basis functions obtained after performing the PCA on each channel's artifact segment. Before the application of this algorithm, initial MR triggers were modified for taking into account of the first stabilizing dummy scanners, which result in an improved performance of the removal.
In figure 25, it is shown, for one channel, a gradient artifact corrupted EEG signal and the cleaned version of the same EEG signal.

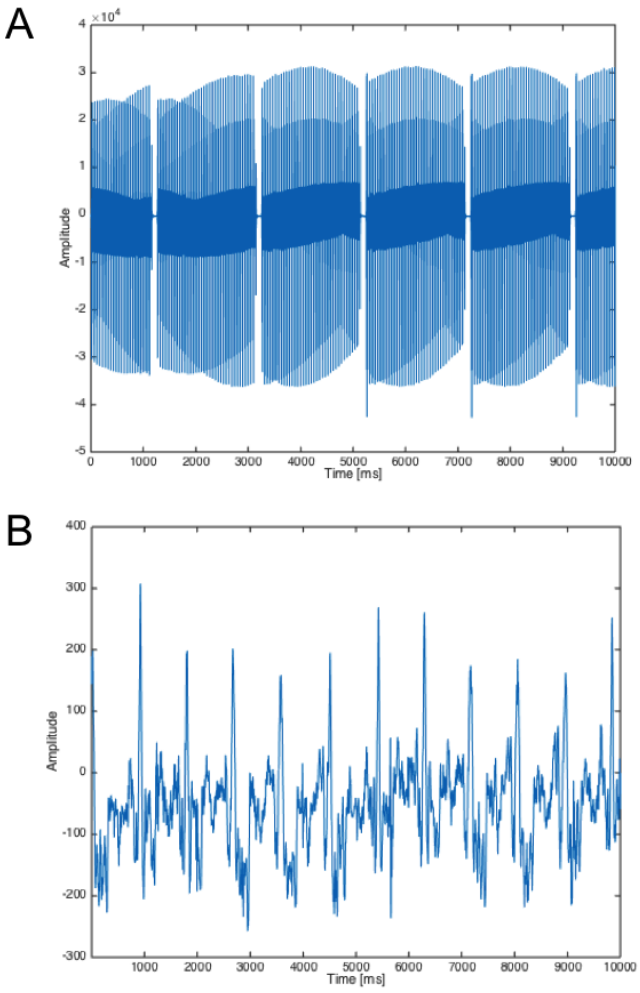

Figure 25 Example of 10 s EEG trace from one channel of one subject A) before the imaging artefact removal and B) after the application of the method for imaging artefact removal

3.2.2 Identification of R peaks in ECG signals

As described in chapter 2, the BCG artefact is related to the cardiac activity of the subject. Therefore, QRS complex identification in the ECG recordings is a critical issue for removing this artifact [25, 30]. In the magnetic field also the ECG signal can be distorted [29]. It is not always possible to identify perfectly the QRS complex. Usually the focus is on the R-peak, since it is the largest and easiest peak to be detected consistently. Finding the R-peaks in the ECG allows identifying the BCG occurrences in the EEG signals.

Before the R-peaks detection, the ECG recording is pre-processed. The pre-processing is composed by the following two steps: 1) band-pass filtering and 2) normalization. The filtering stage is performed by using a FIR band pass filter, realized with Hanning window,

with a low cut-off of 5 Hz and high cut-off of 20 Hz. Filtering the ECG signal allows to highlight QRS complex and achieve a more accurate detection.
The normalization is performed using the z-score normalization, defined as:

$$X_{norm} = \frac{X - mean_X}{\sigma_X} \qquad (3)$$

Where:

- X is the signal to normalize;
- $X_{norm}$is the normalized signal;
- $mean_X$is the mean value of X;
- $\sigma_X$is the standard deviation of X.

It is performed because signals from different subjects can have different amplitudes and the normalization allows to work with a more homogeneous dataset.

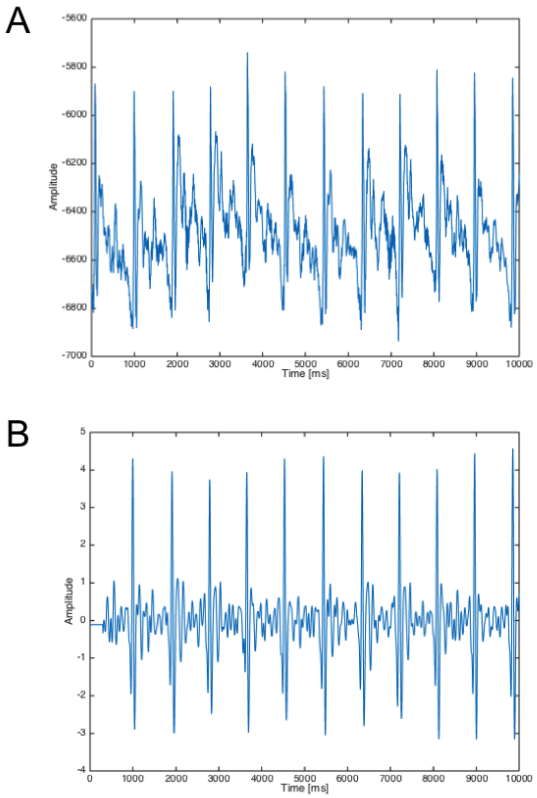

Figure 26 Initial 10 s of ECG signal recorded on subject 1 A) before and B) after the pre-processing steps.

The processed ECG is a signal of better quality, as showed in figure 26 A, thus the R peak is easier detectable (fig. 27).

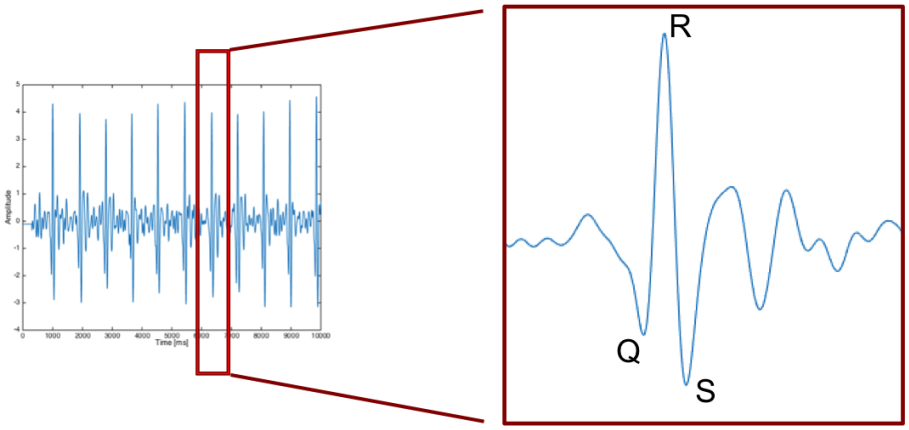

Figure 27 Magnification of one QRS complex on ECG trace in fig 28. The three waves, in this case are clearly recognizable.

The R-peak detection algorithm is based on time and amplitude thresholds. The detection is performed through the use of the *findpeaks* built-in Matlab function.
In order to detect the right peaks, the minimum value of peaks height is set up equal to 1.5 (the signal is normalized), which means that the algorithm detects only the peaks higher than 1.5. The minimum value for the time distance, instead, is set up equal to 600, which means that the algorithm detects peaks with a minimum distance between each other (the so called RR interval) of at least 600 ms (it corresponds to 100 beat per minute). The time threshold has been chosen equal to 600 ms because this is an experimental RR interval for a resting state condition. The output of this algorithm gives the positions in time, along the ECG signal, and the height of each R peak. In figure 28, an example of ECG trace with the detected peaks is illustrated.

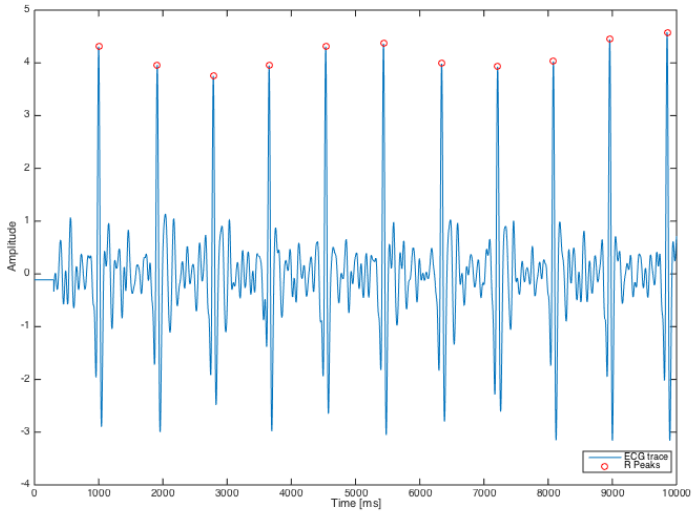

Figure 28 Initial 10 s of the ECG trace from subject 1 with the detected R peaks (red circles)

3.2.3 Identification of BCG peaks in EEG signals

It is generally accepted that EEG signals must be re-referenced in order to remove the inevitable residual neuronal activity in the physical references (as Cz) [37]. The re-referred signals are calculated as:

$$EEG_{Re-ref} = EEG - EEG_{ref} \quad (4)$$

where EEG are the original acquired data, EEG_{ref} is the reference signal (evaluated as the mean of EEG signals across channels) and EEG_{Re-ref} is the re-referenced signal.

As mentioned before, for this study the EEG data were recorded by using the 256 high-density EEG net by EGI. Since the Cz electrode is a reference electrode and does not measure any potential, in order to evaluate the Cz referred signal we need to subtract the reference signal to zero. Therefore, the Cz referred signal is equal to the reversed average EEG signals (4).

This signal is processed in the same way of the ECG signal: band pass filtering and normalization. In figure 29, the comparison between the no-processed Cz referred signal and the processed one is illustrated.

The Cz referred signal describes the average recorded neuronal activity. It has been chosen as representative of the BCG artefact occurrences in order to make comparison between subjects. This is possible because the Cz position is a common position for all the subjects,

it is used as reference for positioning the net. Thus on this signal, for each subject, the BCG peaks have been identified.

Unlike the ECG signals, detecting BCG peaks on this signal is unfortunately more difficult because each BCG artefact occurrence is composed by different peaks. Some of them are spurious peaks. Thus, for this challenging goal, it has been implemented a specific algorithm. The algorithm is composed by these steps:

- estimation of a global time delay between the R peaks and the BCG occurrences;
- epoching of Cz referred signal;
- evaluation of average Cz referred signal;
- research of BCG peaks on the Cz referred signal epoch by epoch.

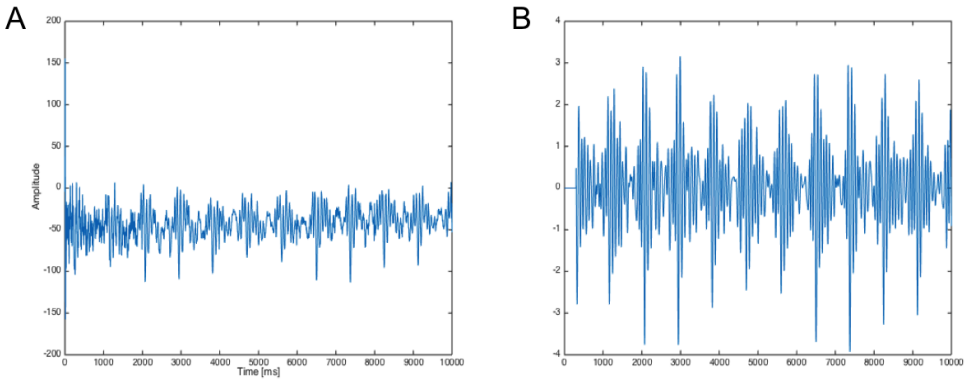

Figure 29 Initial 10 s of Cz referred signal of subject 1 A) before and B) after the pre-processing steps.

What we know about BCG artefact is that its highest contribution appears after a certain delay from the R wave. This contribution is related to the blood flow from the heart to the head and it is delayed of a certain time after the systolic ejection [29].

Thus, to understand the entity of this delay, a cross-correlation between the ECG signal and the Cz referred signal is performed. The lag in correspondence of the maximum value is considered as the time delay, with the hypothesis that acceptable values should range between 150 and 300 ms [29, 30]. The maximum value of the cross-correlation, due to the very different shape of Cz referred signal compared to the ECG signal, does not match the hypothesis for all the subjects. For those subjects the delay was estimated manually by visual inspection of the Cz referred signal and the ECG signal.

The time delay previously estimated represents an average value of the BCG artefact delay and it is used in the algorithm in order to identify the research interval of BCG peaks on the Cz referred signal. We will refer to it as global time delay.

In the first parte of the algorithm the epoching of Cz referred signal is implemented. This approach consists in “cutting” the signals in epochs. An epoch, or trial, is a time window containing a specific number of samples. The epochs are identified using triggers.

The Cz referred signal is epoched in segments of a specific length, by using the ECG peaks as triggers. The length has been chosen equal to 601 ms because these is the minimum RR interval in resting state. These epochs are averaged, obtaining an average Cz referred signal.

In the second part of the algorithm, the detection of the BCG peaks is performed epoch by epoch, in a time window of 60 ms centered on the global time delay previously calculated. The output of this algorithm gives: the position in time, along the Cz referred signal, and the height of each BCG peak.

In figure 30, an example of Cz referred signal with the detected peaks is illustrated.

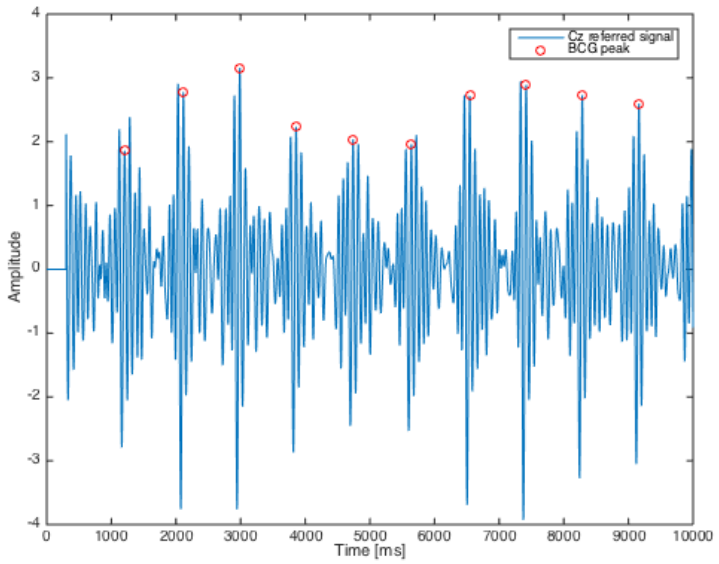

Figure 30 Initial 10 s of Cz referred signal of subject 1 with the detected BCG peaks (red ring). It is possible to notice the presence of different peaks for each occurrence of BCG artefact.

3.2.3.1 Statistical Analysis of RR interval and R-BCG delay relation

Following the previous processing, the information on the location of the R peaks and the BCG peaks on the ECG and Cz referred signal, respectively, is known. The statistical analysis is performed to better understand the relation between the cardiac pulsatility and the delay between the R peak and the correspondent BCG peak.

The first step consists in the evaluation of the heart rate variability, which describes how the RR interval changes across time along the ECG recording. To this end, we perform the difference between consecutive locations of R peaks. The second step is based on the evaluation of beat-to-beat delay of each R-BCG. This information is obtained by performing the difference between the location of R-peak and the position of corresponding BCG peak.

The Tukey's method [39] is used to remove outliers in the R-BCG delays vector, defining as outliers the values:

- below 1^{st} Quartile $- 1.5 \times IQR$
- above 3^{rd} Quartile $+ 1.5 \times IQR$

Where IQR is the interquartile range. If outliers are identified, they are excluded and the evaluation of the correlation between the RR intervals and the R-BCG peaks delay is performed. The correlation is calculated intra-subject and inter-subjects.

3.2.4 Epoching and averaging of EEG signals

The epoching of EEG signals is a widely used approach for studying BCG artefact. This approach consists in "cutting" the EEG signals in epochs, channel by channel. An epoch, or trial, is a time window containing a specific number of samples. The epochs can be identified using ECG peaks. In this way, the signal is divided in a number of epochs equal to the number of heartbeats and in each epoch there will be the BCG artefact related to that specific beat.

First of all, the EEG signals are re-referenced (4). Then, the EEG signals obtained are epoched, using ECG peaks, in trials with length of 601 ms. With an iterative procedure across channels, the signal is divided in trials by giving as starting instant the location of current R peak. In figure 31, an EEG trace with some identified epochs is illustrated. The

red lines are drawn in correspondence of each R peak, which is the starting instant of the EEG epoch. In figure 32, the shape of the first epoch is shown as example.

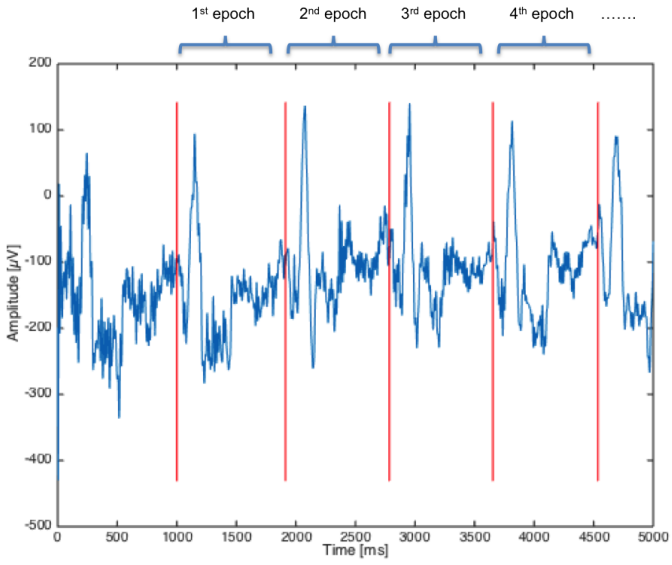

Figure 31 Initial 5 sec of EEG signal of channel 54 in subject 1 with the first four epochs identified by R peaks of ECG trace

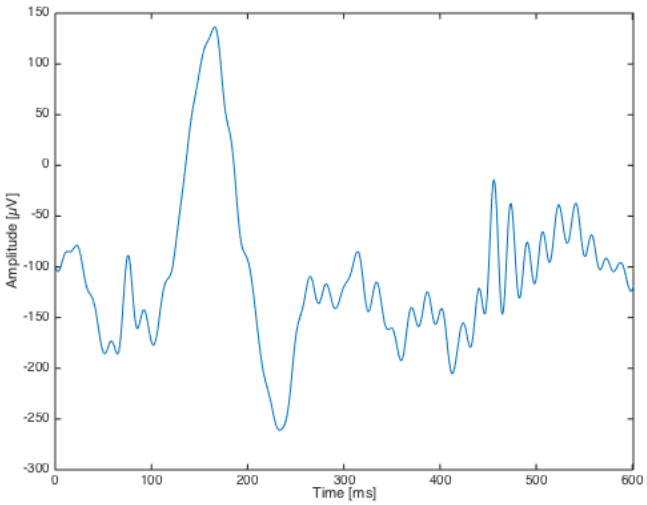

Figure 32 The first epoch of EEG signal of channel 54 in fig. 31

The epochs are averaged and an averaged and epoched signal is obtained for each channel. This average signal describes the global dynamic of the BCG signal in the specific channel. In figure 33A all the epochs of a channel are illustrated and this representation is also called butterfly plot. Butterfly plot is another way to call the epoched data.

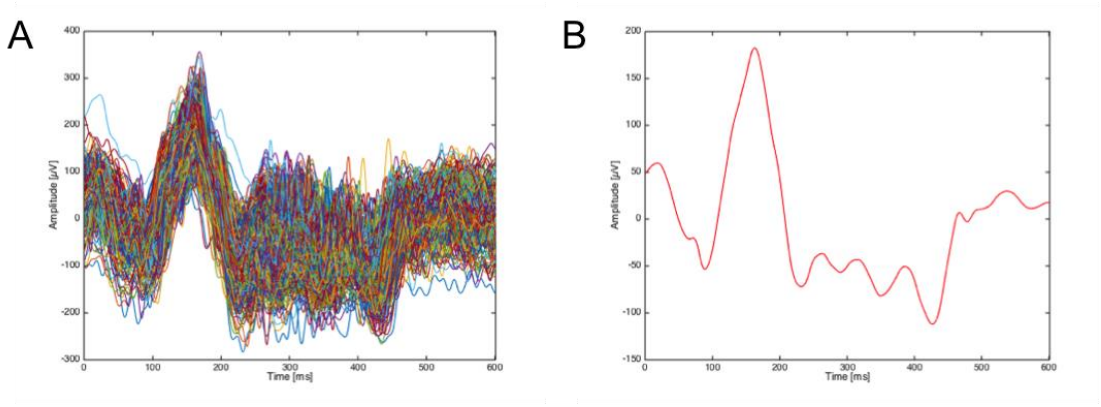

Figure 33 A. Butterfly plot of all epochs of channel 54 of subject 1; B. Average of epochs in A and this signal has been calculated for each channel.

In the next section, the average EEG signals will indicate the matrix containing averaged and epoched signal calculated for each channel: a 256x601 matrix, in which rows represents the channels and columns the time-length of the epochs.
In figure 34, an example of butterfly plot of average EEG signals is illustrated.

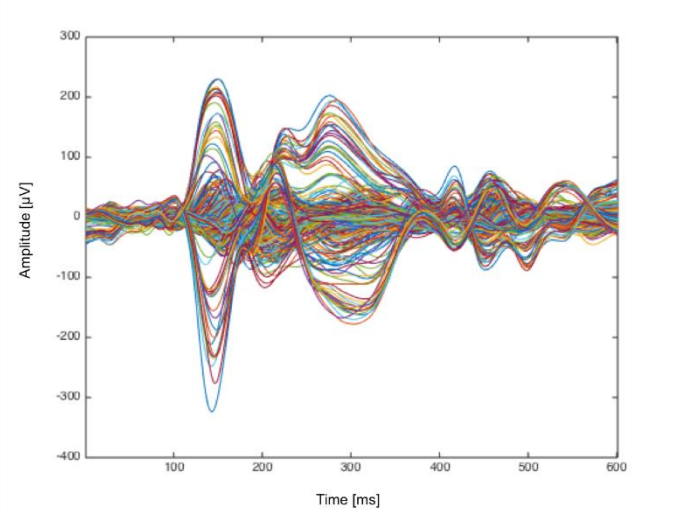

Figure 34 Butterfly plot illustrating the EEG signal of subject 1 of each channel epoched and averaged previously

3.2.5 Evaluation of root mean square of EEG signals

The average EEG signals obtained by the previous steps can describe the average dynamic of the BCG artefact in recorded EEG data. We calculated the power of the epoched data by using the root mean square (RMS) of the average EEG signals across channels.
The root mean square is defined as:

$$X_{RMS} = \sqrt{\frac{1}{N}\sum_{n=1}^{N}|X_n|^2} \qquad (5)$$

The X_{RMS}, in this case, is a vector with length equal to 601. Each value derives from the calculation of root mean square across channels for each instant.
The RMS is used because it describes how the power of EEG signals is distributed in time without taking into account the different contribution by different channels, unlike the average EEG signals, which leads to the loss of information in correspondence of opposite peaks in different channels.
On this vector, some peaks can be identified with the hypothesis that in correspondence of these peaks the maximum activity can be identified. In this case, these peaks should describe the contribution of BCG artefact [29].
Following the computation of the RMS for all the subjects, one subject has been chosen as reference.
These peaks have different latencies from the R peak (in this contest the R peak is that one of the average ECG trace, that can be calculated epoching the ECG signal. The delays previously calculated is referred to each occurrences of mean BCG peaks in the CZ referred signal with each R peak in the ECG signal), and they can explain some features of BCG artefact.
Therefore, the values of average EEG signals, of a chosen subject, in the instants that correspond to these peaks, are used as reference to look for common activity across subjects.
In figure 35 an example of RMS is illustrated.

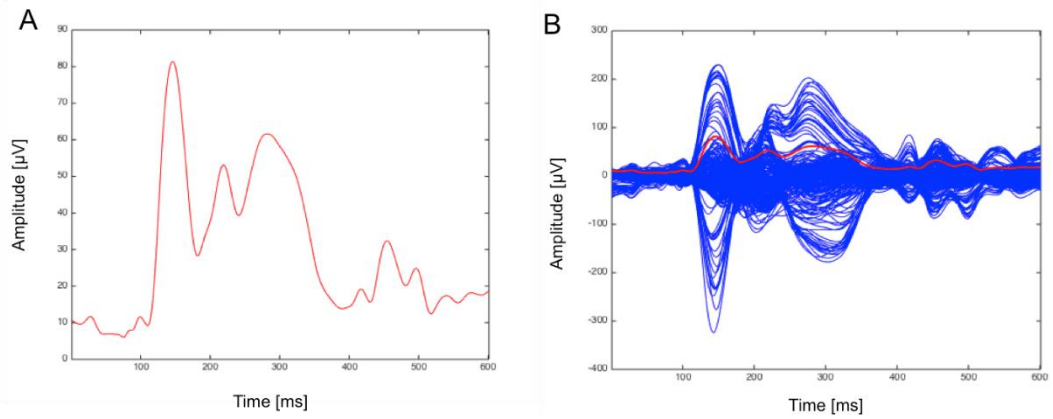

Figure 35 A. RMS of the averaged EEG signals illustrated in fig 34. B. RMS plotted on corresponding averaged EEG signals.

3.2.6 Evaluation of field distribution maps

3.2.6.1 Cross-correlation between maps

The cross correlation is performed with the aim of finding common activity between subjects by creating average topographic maps that allow the spatio-temporal BCG artefact characterization (see fig. 36 as example of topographic map). Specifically, the cross-correlation is calculated between the average EEG signal of reference (in the instants corresponding to the peaks) and the average EEG signal of other subjects. The maximum value of the cross-correlation identifies the instant in which the activity is similar across subjects. In this way, each subject is characterized by the same number of instants in which the average EEG signal shows similar activity distribution on the scalp with all the other subjects.

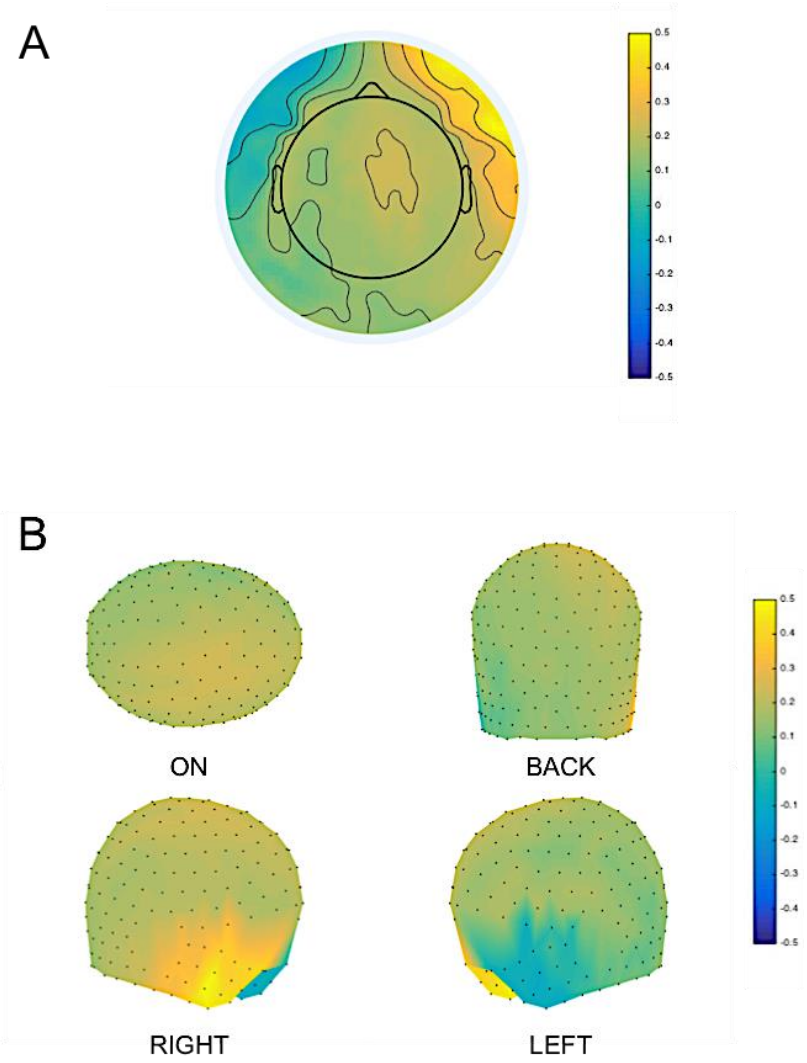

Figure 36 In this figure an example of topographic map of EEG signal is illustrated. The maps describe the EEG signal in a defined instant in each channel. The black points indicate the electrodes location.

In order to compare the activity across subjects, the average EEG signals are scaled between -1 and +1 with the following definition of normalization, called min-max normalization:

$$X_{norm} = \frac{X - min_X}{max_X - min_X} \times (new_{max_X} - new_{min_X}) + new_{min_X} \qquad (6)$$

Where:

- X is the signal to normalize;
- $X_{norm}$is the normalized signal;
- min_X is the minimum value of the signal;

- max_X is the maximum value of the signal;
- new_{min_X} is the minimum value of normalized signal (in this case -1);
- new_{max_X} is the maximum value of normalized signal (in this case +1).

Average maps are created averaging the EEG signals of all subjects in correspondence of instants previously evaluated. Thus, for each of these instants an average map is created and in practice this map is a vector (length equal to the number of channels, 256) composed by 256 values, each one describing the average activity in a specific channel for that specific instant.

3.2.6.1 PCA of average maps

The Principal Component Analysis (PCA) is performed across subjects (on selected time instants) in order to find the main contributions to the activity of BCG artefact. It is implemented using the *pca.m* built-in function, which gives in output the principal components with the associated variance and the weights to reconstruct the data using the principal components.
The inputs of the PCA are the average maps previously found and the outputs are principal components organized with decreasing variance. The principal components can help to understand which are the main contributions to the BCG artefact.
These components are vectors composed by 256 values (one for each channel) thus it is possible to inspecting them as maps across the scalp.

Chapter 4 – Results & Discussions

In this chapter the results obtained applying the methods described in the previous chapter will be shown. Specifically, the results obtained by the statistical analysis of RR interval and R-BCG delays are described with some observations and discussion. Successively the results and comments referring to the characterization of BCG activity are reported.

4.1 Relation between RR interval and R-BCG delay

The detection of R peaks in the ECG signal as well as that of the BCG peaks in the Cz referred signal allows a better understanding of the relation between the cardiac frequency of a subject and the occurrence of its BCG artefact. From previous studies [27, 29, 38] the correspondence of BCG artefact to the cardiac activity was addressed.

Here we want to understand how the occurrence of BCG artefact is related to the heart rate changes. For reaching this goal the R-BCG peaks delay has been calculated and also the heart rate variability (HRV) has been estimated to describe the variation of cardiac frequency along a recorded signal.

The evaluation of R-BCG delays was reported also in the study by Iannotti et al [38], in which they found that the BCG artifact is delayed compared to the ECG events. This latency is not perfectly constant within a subject and it varies across subjects.

In figure 37, the results of the statistical analysis about the relation RR interval of ECG signal with the R-BCG delays are illustrated for subject 1.

The detection of BCG peaks for subject 6 was not successful, due to the presence of spurious peaks in the Cz signal. For this reason, this subject was excluded for this first analysis. However, since the R peaks detection from the ECG signal for this subject was accurate, we could use it for the second part of the work, as the epoching of EEG data was based on the ECG peaks.

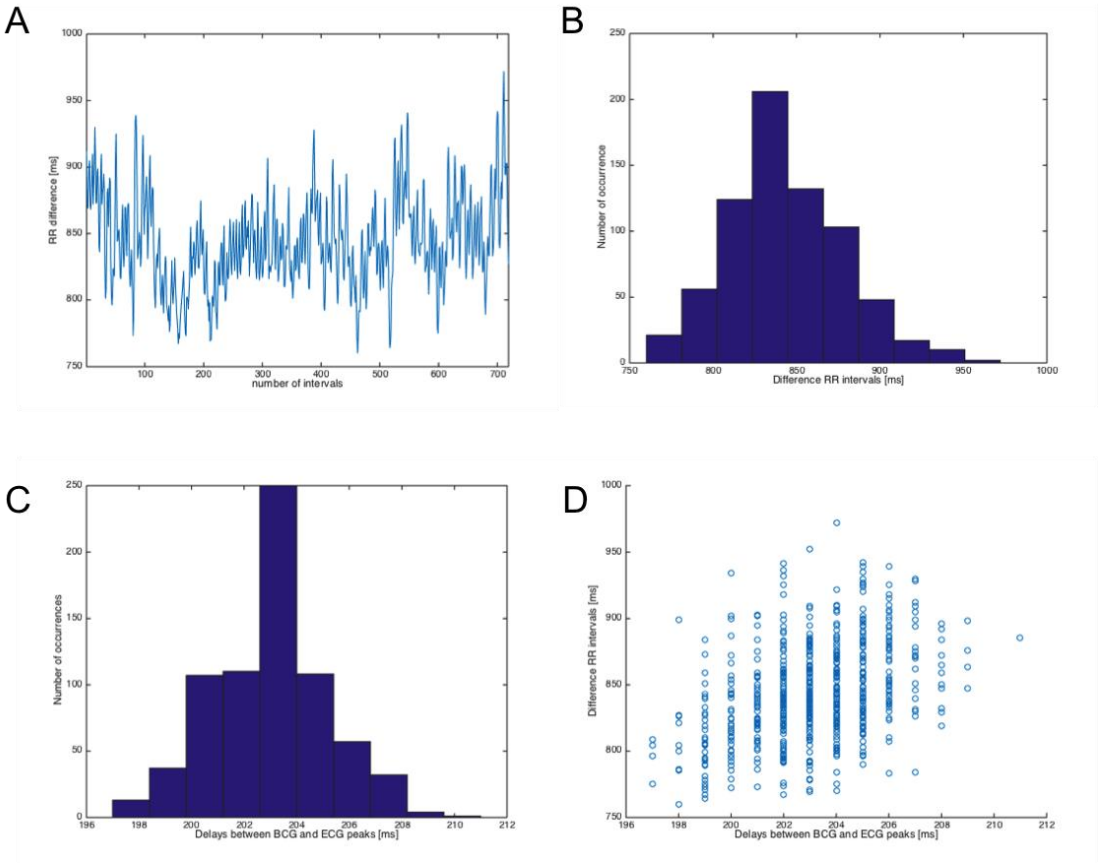

Figure 37 A. Heart Rate Variability (HRV) of subject 1. On the y-axis the time difference between RR peaks is shown. On the x-axis there are the referred intervals. B. Histogram describing the distribution of time difference between RR peaks. C. Histogram describing the distribution of R-BCG delay. D. Scatter plot describing the relation between RR interval and corresponding R-BCG delay.

The numerical results for all subjects are reported in Table 2.

Table 2 In this table the values of RR intervals, R-BCG delays and Pearson's correlation coefficient of these two quantities are summarized

	R-R interval duration [ms]	**R-BCG peaks delay [ms]**	**Pearson's correlation coefficient (intra-subject)**
Subject 1	843.69 ± 34.63	203.13 ± 2.24	0.38
Subject 2	957.54 ± 61.32	187.83 ± 2.63	0.15
Subject 3	1085.60 ± 48.80	261.11 ± 3.04	0.30
Subject 4	975.61 ± 57.91	198.56 ± 4.45	0.02
Subject 5	946.55 ± 74.13	158.56 ± 2.77	0.10

By looking at table 1 it can be observed that the HRV shows different values between subjects with a minimum value of 843.69 ± 34.63 ms for subject 1 and maximum value of 1085.60 ± 48.80 ms for subject 3. The average and the standard deviation values are both in a normal range.

About the R-BCG delay, large variability across subjects can be observed, with a minimum value of 158.56 ± 2.77 ms for subject 5 and a maximum value of 261.11 ± 3.04 ms for subject 3, with an average difference of about 100 ms. At the same time, low intra-subject variability can be observed with low standard deviation.

The intra-subject correlation between the RR intervals and the R-BCG peaks delay shows a positive trend. A large range of correlation values is covered across subjects, e.g subject 1 is characterized by a correlation coefficient 0.38, whereas subject 4 is characterized by a correlation coefficient 0.02, maximum and minimum values respectively.

The positive correlation indicates that when the RR interval increases (or rather the cardiac frequency decreases, i.e. less number of beats per minute) also the R-BCG delay increases. In other words, when the cardiac activity decreases in rate, the BCG artefact appears with a larger delay after the R wave.

This could be explained by the fact that the cardiac frequency increases when the sympathetic nervous system is active and it constricts blood vessels. The blood flow rate is equal to the multiplication between blood velocity and the area of the vessel section. If the area decrease (due to the action of sympathetic nervous system) the velocity increase to ensure the same flow rate. An increasing blood velocity could mean a reduction of the delay between the BCG occurrence and the R wave. This is a very simple explanation that does not take into account of different factors, like the blood pressure and the position of the subject (lying on table scanner). Thus further investigation should be performed.

For investigating the general trend of the RR interval and R-BCG peaks delay relationship, the Pearson's correlation coefficient was calculated also across subjects. In figure 38, the results are illustrated.

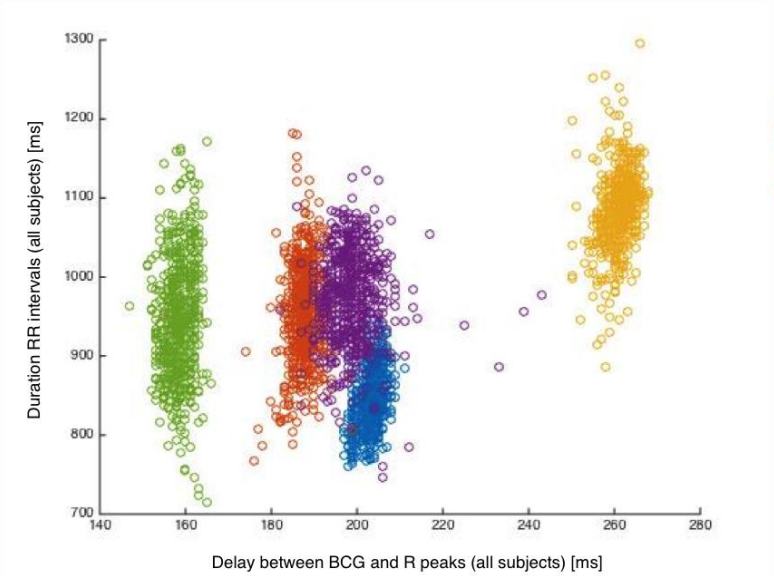

Figure 38 Scatter plot with all subjects, describing the relation between RR interval and corresponding R-BCG delay

The Pearson's correlation coefficient calculated across subjects is 0.47 ($p < 0.05$), which reinforces the positive correlation between the RR interval and the R-BCG delay that was already found at the level of single subject.

These results prove that the occurrence of BCG artefact within a subject is variable. The variability is very large also between subjects. Thus, the use of constant BCG delay for the calculation of artefact template [25, 30] leads to a sub-optimal removal of the artifact, confirmed by the presence of artefact residuals in the clean signal.

In figure 39, the EEG trace of a subject is shown with the ECG trace of the same subject. The high beat-to-beat variability of the BCG artefact, in waveform, amplitude and duration can be observed. In figure 40 the epoched signal related to the same interval of figure 39 is illustrated. It is clearly visible that the waveforms are different between epochs.

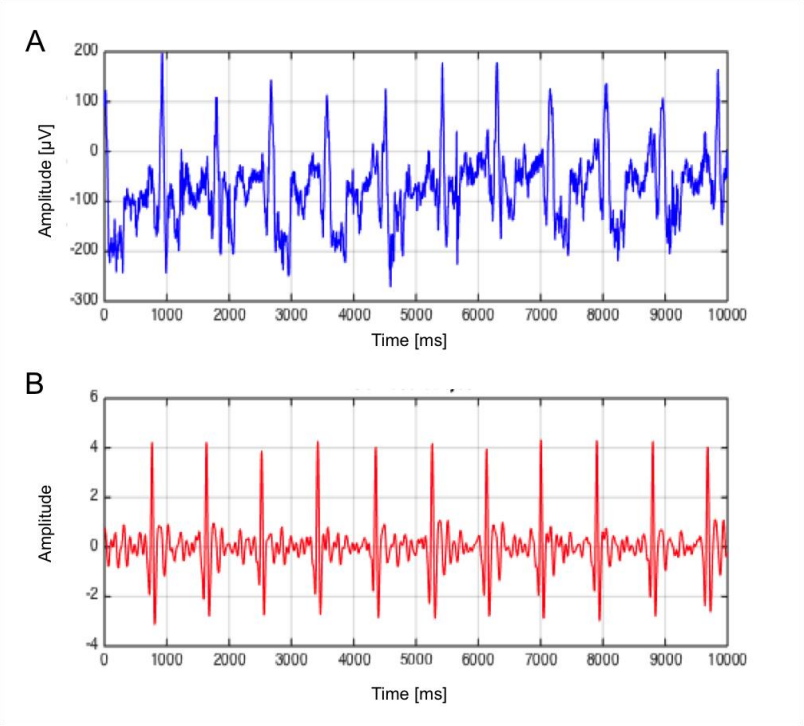

Figure 39 A. 10 sec of EEG signal in channel 54 of subject 1. B same interval in A) of the ECG signal of subject 1. For each R peak in the ECG there is a corresponding BCG peak in the EEG signal. The BCG artefact is characterized by high beat to beat variability, in terms of amplitude, delay and waveform.

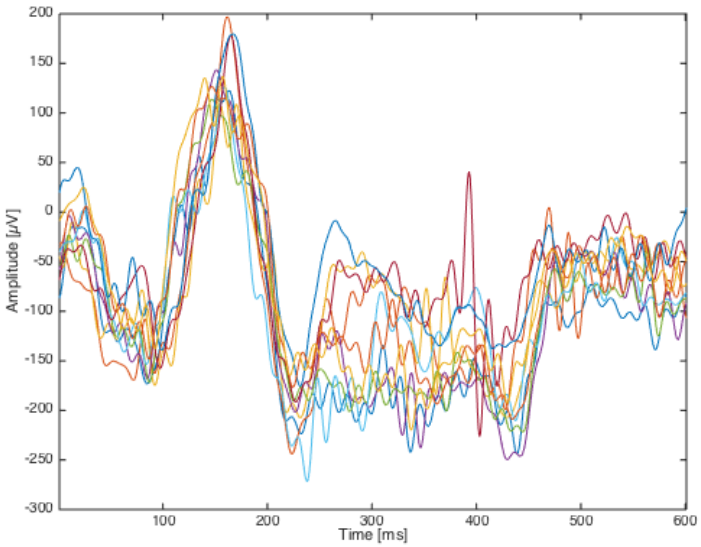

Figure 40 Epochs obtained by epoching signal in fig. 39. The beat-to-beat difference of BCG occurrence is clearly visible.

4.2 Evaluated RMS of EEG signals

Once the average EEG signals have been calculated for each subject, the RMS was calculated on these signals, in order to obtain global information about the time distribution of BCG activity.

In figure 41 A-F each panel illustrates the RMS of each subject.

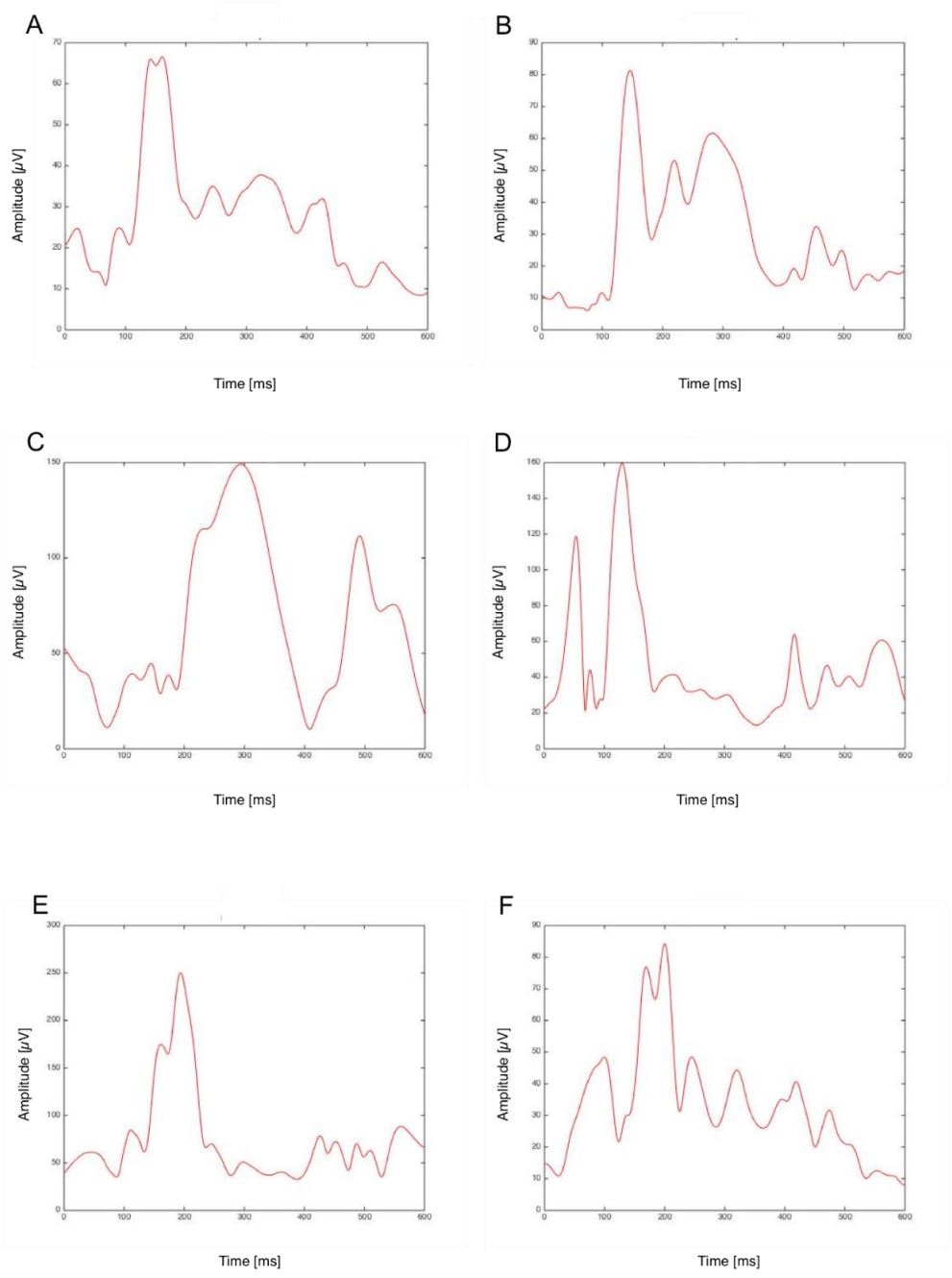

Figura 41 A) RMS of subject 1. B) RMS of subject 2, C) RMS of subject 3, D) RMS of subject 4, E) RMS of subject 5, F) RMS of subject 6. Each RMS is composed by different peaks that describe how the power of BCG artefact is distributed in the time course.

By looking at figure 41, it results that the activities across different subjects are quite different, in terms of: number of peaks, latencies of these peaks, duration and waveform. Indeed, for every subject, the RMS is characterized by several peaks, between which one is usually larger in amplitude and duration than the others.

However, some similarities can be found performing an analysis across subjects. As reported in some previous publications [27, 28, 29] several peaks on RMS can be associated to the contribution of BCG on EEG signals. Each peak is supposed to describe different kinds of contributions, like pulse-driven expansion and pulse-driven rotation movements. Debener et al. [29] affirmed that probably the major peak can be associated to the head rotation contribution.

Since the aim is to find common activity patterns across subjects, the RMS of subject 2 was chosen as reference for the evaluation of peaks associated to the BCG artefact. Five peaks have been identified for performing comparison across subjects. We found that the selection of the peaks in our study is in accordance with the ones in previous works in literature [29]. The instants in correspondence of these five peaks have been used to cross-correlate the average EEG signals of subject 2 (in correspondence of these five instants) and the EEG signals of other subjects.

In figure 42 the RMS and selected peaks are illustrated for subject 2.

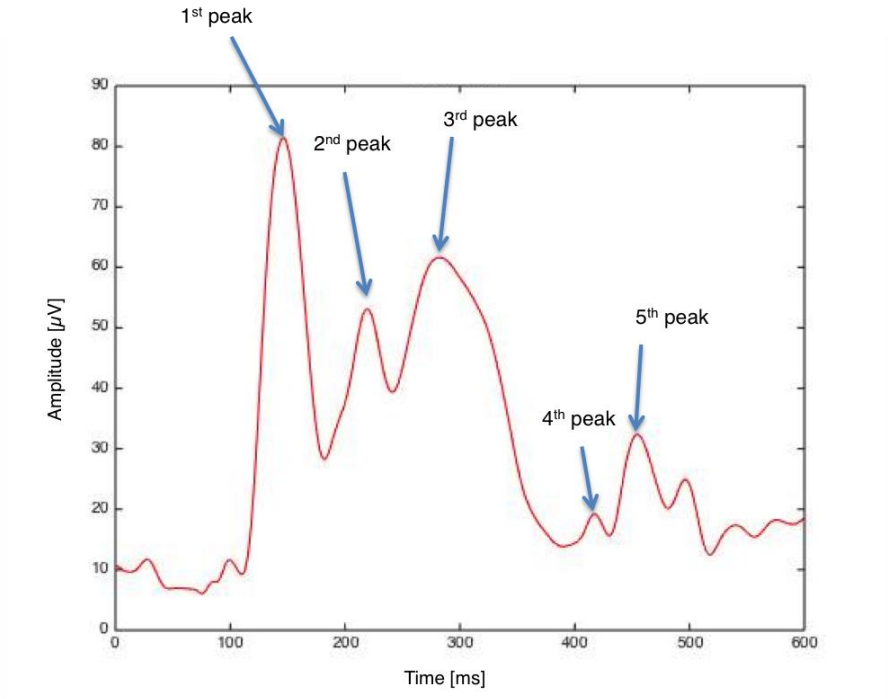

Figure 42 RMS of subject 2, the arrows show the detected peaks

4.3 Results from cross - correlation between maps

Common activity between subjects has been identified in five instants (for each subject), correlating the average EEG signals of subject 2 (in correspondence of peaks reported in table 1) with the average EEG of all other subjects.
In figure 43 the electrical activity of each subject for each instant with maximal correlation with subject 2, is illustrated.

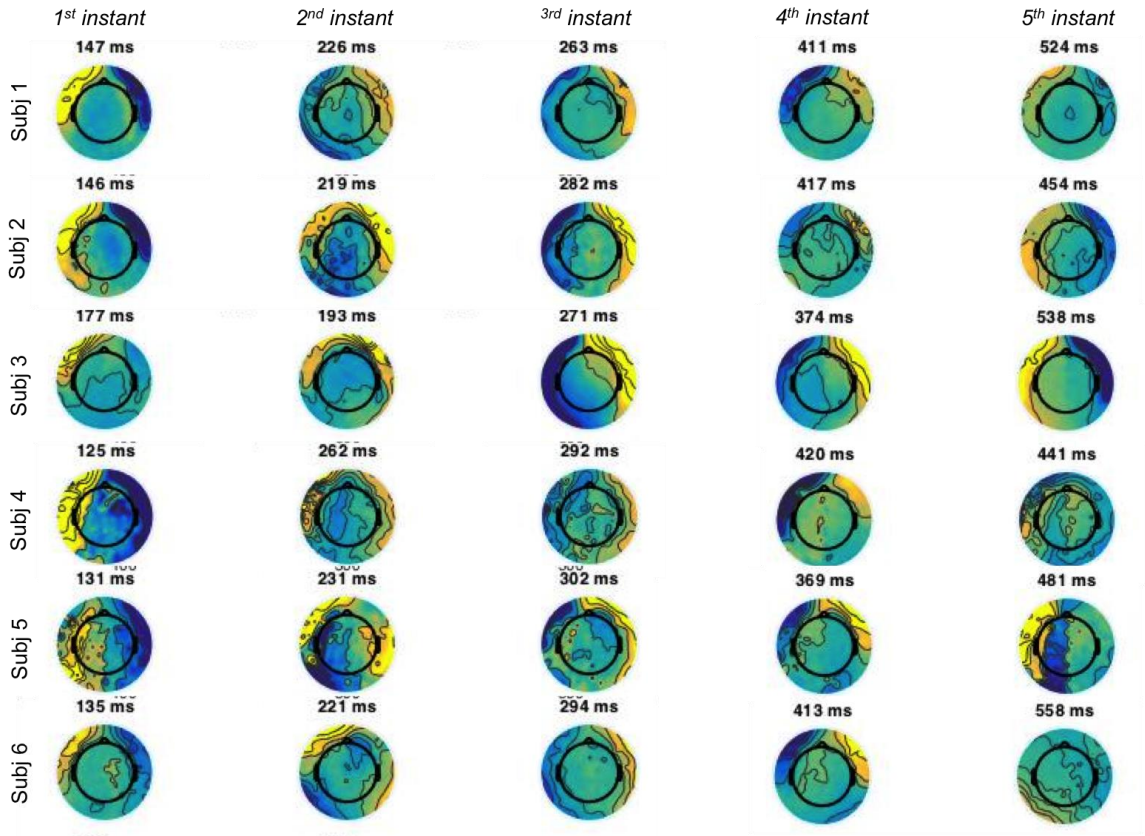

Figure 43 Maps with maximal correlation. For each subjects, 5 maps have been found in correspondence of a specific time instant.

By looking at the previous figure, it is possible to see that after the cross – correlation analysis, the activity associated to subject 2 has been found also in the other subjects. Furthermore, the identified instants belong to similar intervals across subjects.

After the normalization between -1 and +1, the average maps across subjects in correspondence of each instant have been calculated, performing the average between the EEG signals of all subjects in the specific instant.

In figure 44, all the maps are illustrated, in correspondence of the five instants and on four view of the scalp.

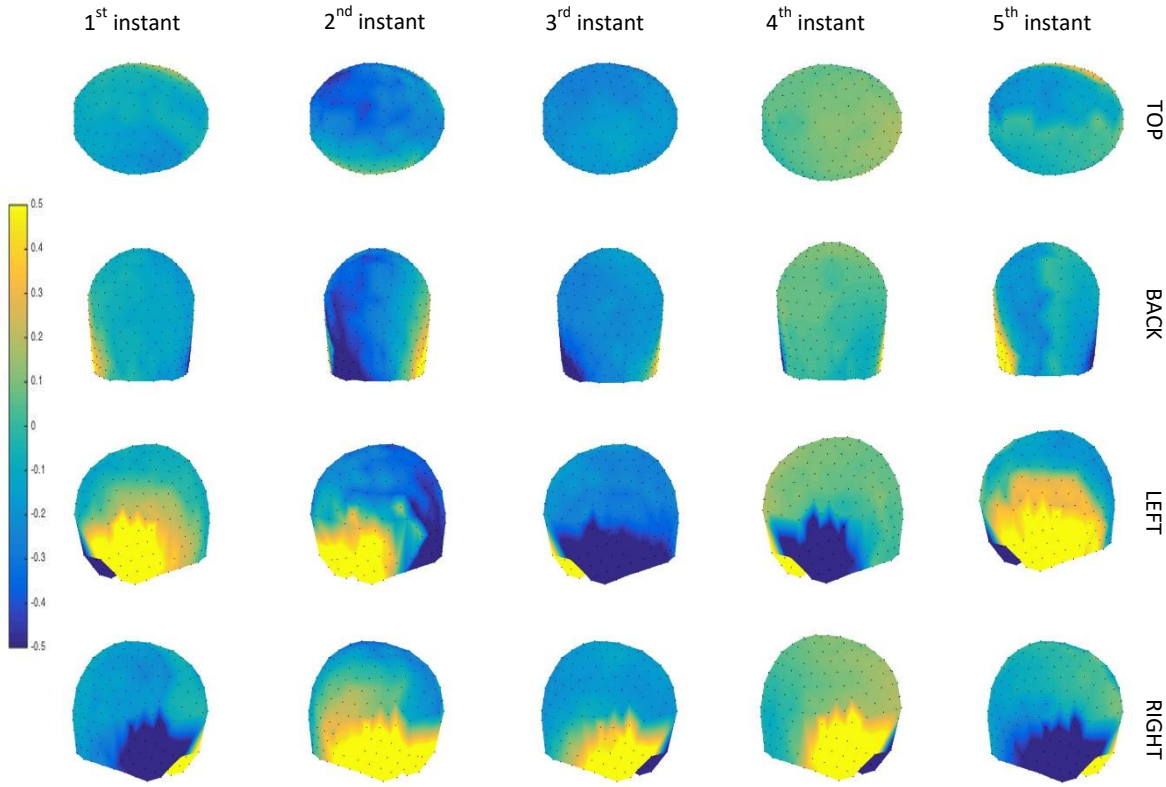

Figure 44 Average maps describing the scalp activity in correspondence of each instant. Four different views of the scalp for each instant are illustrated in each row.

In the table 3, a comparison between the latencies of the detected peaks in the current and in a previous study [29] is reported. The latency is referred to the ECG, specifically considering the R peak of the average ECG signal in correspondence of the RMS zero point because the EEG signal was epoched by ECG peaks.

Table 3 Latencies of the peaks identified by cross-correlation between subject 2 and other subjects. In the last row the latency found in the reference study are reported.

	1st Instant	2nd Instant	3rd Instant	4th Instant	5th Instant
Latency [ms] Current study					
Subject 1	147	226	263	411	524
Subject 2	146	219	282	417	454
Subject 3	177	193	271	374	538

Subject 4	125	262	292	420	441
Subject 5	131	231	302	369	481
Subject 6	135	221	294	413	558
Latency [ms] Reference study [29]					
	176	228	332	440	464

It is important to underline that there are some non-negligible differences between our dataset and the dataset used by Debener et al. The signals used by Debener et al. were acquired with a non-high-density cap (using 32 channels) in a magnetic field of 1.5 T instead of 3 T, as in our study.

Looking at the average maps, it is possible to assert that the BCG affects the EEG signals in a consistent way between subjects.

Specifically, we can observe that different peaks compose the BCG artefact. The peaks show different polarity between the left and right sides of the head and this polarity turns upside down across time.

Looking at the scalp map, opposite intensities of the signals are displayed on the two hemispheres of the head. The polarity reverses across the recording and its negativity/positivity depends on the magnetic static field direction, which is in agreement with previous findings described by Debener et al and Yan et al [27,29].

In particular the polarity is opposite in the first, third, fourth and fifth instant and it reversed from one peak to another. In correspondence of the second instant the left and right hemispheres are characterized by activity with same polarity.

The changing polarity may be due to the rotation of the head caused by the pulsation of blood. A first rotation, after the systolic ejection, causes a peak with opposite polarity on the two sides of the head [29]. Then, it could be followed by a second rotation in the opposite sense, following the backward head movement to the initial position, which causes a polarity reversal between left and right hemisphere. Further contributions may be associated to the expansion of the scalp in correspondence of major vessels, as discussed more in detail in the next section.

The scalp voltage topologies also revealed a relevant feature of the BCG artifact, which consists in its non-stationarity in time. If the BCG artefact showed a stationary pattern, the topoplots would be characterized by homogeneous voltage changes across the full scalp. Whereas, our results show that the activations are uneven in time and space across the scalp.

From these findings it is possible to understand why ICA based methods can lead to the presence of residual artefact even if a good number of independent components is identified. We have demonstrated that the BCG artefact is a non-stationary signal thus the ICA cannot remove it because the basic assumption of non-stationary sources is not satisfied.

4.4 PCA Results

The PCA was performed on the five average maps previously showed (from fig. 44) in order to identify the main contributions to the BCG artefact. Thus five principal components have been calculated. In table 4, the variance associated to each component is reported.

Table 4 Variance of each component obtained by principal component analysis

	Variance (%)
1st Principal Component	69.36
2nd Principal Component	25.76
3rd Principal Component	3.49
4th Principal Component	0.91
5th Principal Component	0.47

Among the five components obtained, only the first two are characterized by a high value of variance. These two components can explain about the 95% of the information carried out by the five average maps. The other three components have a negligible variance.
For the first two principal components the activity was reconstructed by separately considering the two components and focusing on the feature of the representative signal obtained; the scalp maps have been derived to understand how their contribution is distributed on the scalp. These scalp maps are illustrated in the following figure.

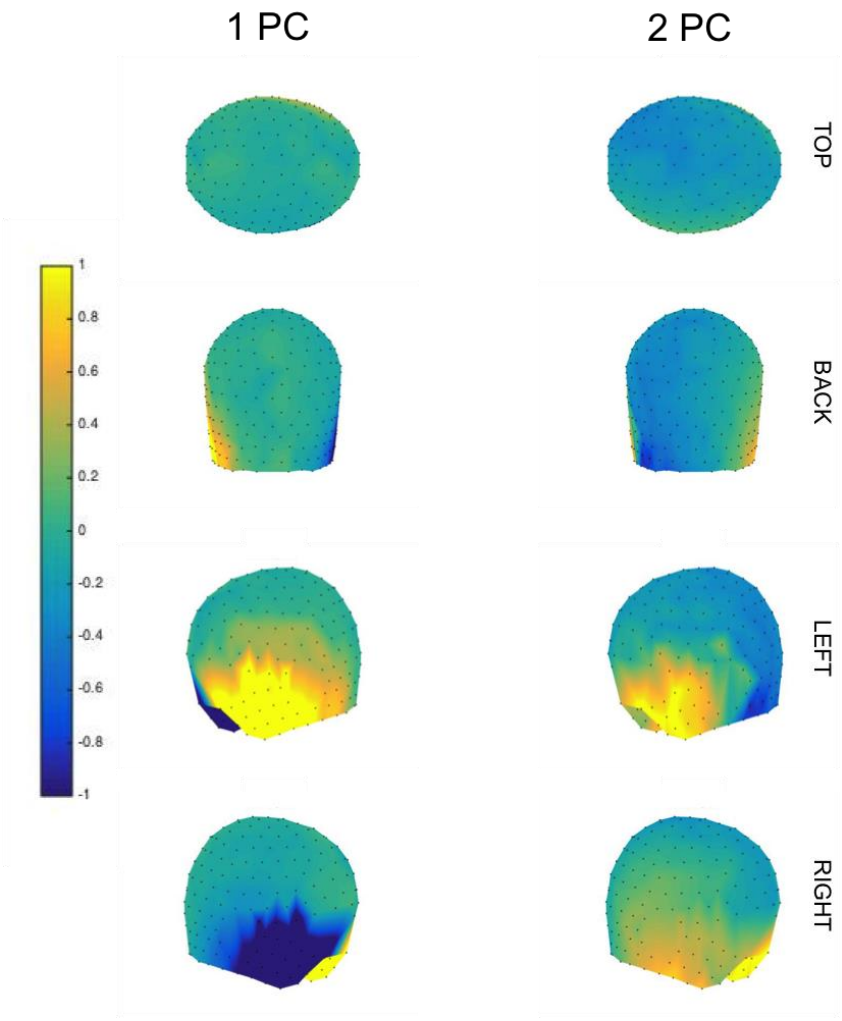

Figura 45 Left panel: distribution maps of the first principal component. Right panel: distribution maps of the second principal component

By performing the PCA, two main contributions to the BCG artefact have been identified. The first principal component is characterized by opposite values between left and right sides of the scalp (see fig. 45). This component should describe the contribution associated to blood flow that can cause the head rotation and Hall effect. Other studies affirm that the head rotation could give the major contribution to the artefact [27,29]. Yan et al. studied the different contributions comparing the result obtained applying a mathematical model with in vivo measures. In particular they estimated the correlation between the BCG artefact and the artefact caused by the only rotation of the head, obtaining a value equal 0.87. This means that the head rotation should be the major contribution, but at the same time it is not the only one.

The second component is characterized by positive values on both sides of the scalp with a higher activity on the left side. It should describe the contribution associated to the scalp

pulsation. The scalp pulsation may be caused by pulsatility of the blood in head vessels. The major vessels are the temporal arteries and external carotid arteries, which are located on the left and right sides of the head, thus they could give the major contribution to the scalp expansion. In figure 46 the vessels anatomy of the head is illustrated.

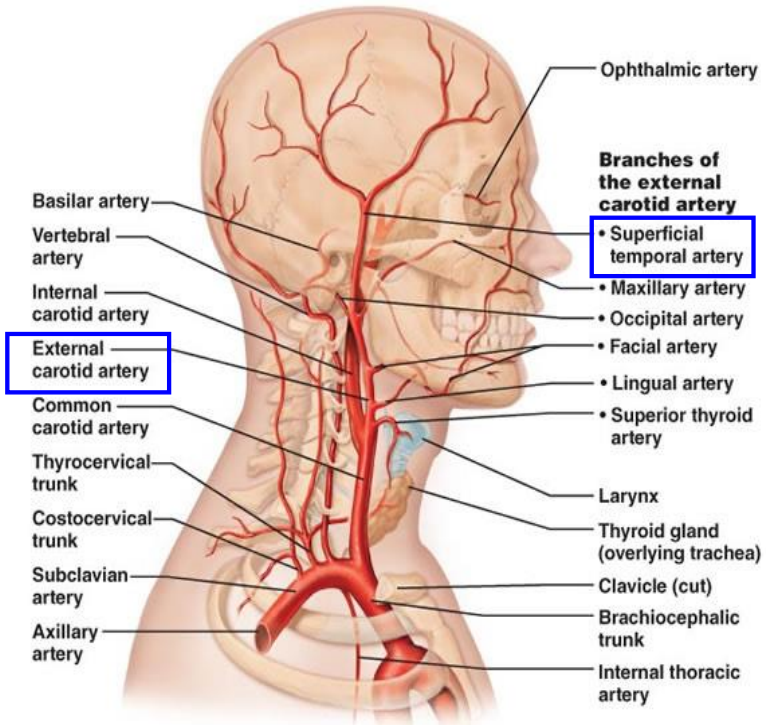

Figure 46 Illustration of artery vessels in the neck and head. The temporal artery and external carotid artery are indicated. This is a representation of the right part, the left one is specular.

Furthermore the higher contribution on the left side could be due to the fact that the blood is pumped from the left side of the heart to the head. Thus the movement driven by the pulsation could be larger.

For all the instants of interest, the activity is higher in correspondence of the cheeks. This could be explained by the fact that the electrodes positioned on the cheeks are less constrained than the other electrodes. In fact as described in section 3.1 an elastic bandage was positioned on the head in order to minimize electrodes movement. Furthermore, the electrodes on the posterior part of the head are constrained also by the head coil and the table, as the subject is lying on it.

Conclusion

The results of our study on BCG artifact characterization revealed that each method proposed for attenuating the BCG can lead to the presence of residuals. Nonetheless, our study provides important information to develop an optimized method based on the artefact's features.

An important finding of our study is the delay between peaks in the ECG and the BCG signals varies between occurrences in the same subject and across subjects. The AAS and OBS methods assume a constant delay to identify BCG occurrences in the EEG signal. From literature, this constant delay is assumed to be 210 ms [30], but we showed that it is actually characterized by very different values, ranging from 160 ms to 260 ms. Neglecting this variability can lead to sub-optimal identification of the BCG events, and, consequently, to a not-perfectly-matched template subtraction.

Furthermore, we have shown that the artefact is characterized by relatively high variability: between occurrences in the same channels, across channels of the same subject and between subjects, not only for the delay values but also for waveform and amplitude. Thus, this can explain why the AAS method, which assumes the reproducibility of the artifact waveform across epochs, has large residuals. As discussed in the second chapter, the AAS method is based on the construction of an average template of the artifact, which is subtracted from the EEG signals. Better removal can be obtained by using the OBS method, which can remove residual artefacts by principal component analysis. On the other hand, as explained before, also the OBS method takes into account of a constant delay between the R peak and the related BCG event. Furthermore, other problems related to OBS methods are associated to the identification of an appropriate number of principal components to construct the basis set.

As mentioned in chapter 2, the ICA procedure is based on the assumption that the signal sources have stationary properties. By displaying the actual distribution of the BCG artefact in time and space (across the scalp), we can assert that this artifact shows non-stationary features. Thus, when using ICA methods, an artefact residual will be always present in the clean EEG signals, as the stationary assumption is not satisfied. Moreover, another limitation of ICA is related to the number of independent components used to describe the BCG artefact. Their number is not fixed and this can cause missing identification or wrong identification of components, thus to the presence of residual in the EEG signals.

In this thesis, the relation between the subject's cardiac frequency and the BCG occurrences has been identified. In particular, we found a positive correlation between the RR interval and the R-BCG delays, which means that to cardiac frequency increases, the R-BCG delay decreases.
Another important finding is about the main contribution to the BCG artefact. Performing the PCA on the average activity obtained across subjects, two main patterns have been found. The first one may be related to blood flow, possibly to the head rotation caused by the axial movements after the heart blood ejection towards the head. The second one may be related to the scalp expansion due to the pulsatility of the blood in the major vessels [27,29].

Starting from our results, further investigations that combine concurrent approaches and technologies could be really useful. The integration of electrical, mechanical, and imaging measurements may permit studying the BCG artefact in a more direct way. In particular new experiments for addressing specific information about the origin and dynamic of the artefact could be conducted, starting from the knowledge about the two principal contributions (head rotation and scalp expansion). For example by directly measuring the scalp movement (by accelerometers) we could directly study the contribution of the pulsatility. Furthermore, physiological information about the blood flow in the brain and in the scalp can be collected to understand more fully the relation between the cardiac frequency and BCG artefact. This information could be extracted by performing fluid dynamic studies, for example by transcranial doppler or cerebral angiography.
In summary, we hope that our findings about BCG artefact will be useful for developing new methods for its removal and as a start point for planning new experiments and studies.

Acknowledgements

Vorrei ringraziare la prof.ssa Cristiana Corsi per la disponibilità e il supporto dimostratomi sin da subito nel voler intraprendere quest'avventura della tesi all'estero.
Ringrazio il prof. Dante Mantini per avermi ospitata presso il Research Centre for Motor Control and Neuroplasticity, dell'università KU Leuven, Belgio.
Inoltre ringrazio i ragazzi del BIND group, in particolare l' Ing. Marco Marino per la sua costante disponibilità.
Non possono mancare i ringraziamenti alla mia famiglia che mi ha dato la possibilità di arrivare a questo traguardo.
Infine ringrazio i miei amici e compagni di corso per le ore di studio, e non solo, passate insieme.

Bibliography

[1] Mulert C., Lemieux L., (2010), "*EEG-fMRI – "Physiological Basis, Technique and Applications",* Springer.

[2] Avanzolini G., Magosso E., (2015), *"Strumentazione Biomedica, Progetto e impiego dei sistemi di misura",* Bologna, Patron Editore.

[3] Song J., Davey C., Poulsen C., Luu P., Turovez S., Anderson E., Li K., Tucker D., (2015), *"EEG source localization: sensor density and head surface coverage",* Journal of Neuroscience Methods 256, 9-21.

[4] Oostenveld R., Praamstra P., (2001)*"The five percent electrode system for high-resolution EEG and ERP measurements",* Clinical Neurophysiology 112, 713-719.

[5] Materials from Bioelettromagnetismo course, prof. A. Costanzo

[6] Ives J. R., Warach S., Schmitt F., Edelman R.R., Schomer D.L.,(1993), *"Monitoring the patient's EEG during echo planar MRI",* Electroencephalography and Clinical Neurophysiology 87, 417-420.

[7] Modo M., Bulte J. W. M., (2011)*"Magnetic Resonance Neuroimaging – Methods and Protocols"*, Springer.

[8] D. Mantini, Perrucci M.G., Del Gratta C., Romani G.L., Corbetta M., (2007), *"Electrophysiological signatures of resting state networks in the human brain"*, PNAS 104, 13170-13175.

[9] Ogawa S., Lee T.M., Nayak A.S., Glynn P., (1990) *"Oxygenation-sensitive contrast in magnetic resonance image of rodent brain at high magnetic field",* Magnetic Resonance Medicine 14, 68-78.

[10] Shmuel A., (1996) *"Functional organization for direction of motion and its relationship to orientation maps in cat area 18",* Journal of Neuroscience 16, 6945-6964.

[11] Mathiensen C., Caesar K., Akgoren N., Lauritzen M., (1998), *"Modification of activity dependent increases of cerebral blood flow by excitatory synaptic activity and spikes in rat cerebellar cortex",* The Journal of Physiology 512, 555-566.

[12] Smith A.J., Blumenfeld H., Behar K.L. Rothman D.L., Shulman R.G., Hyder F., (2002), *"Cerebral energetics and spiking frequency: the neurophysiological basis of fMRI",* Proc Natl Acad Sci USA 99, 10765-10770.

[13] Laufs H., (2012), *"A personalized history of EEG-fMRI integration"*, NeuroImage 62, 1056-1067.

[14] Kilner, J. M., Mattout, J., Henson, R., Friston, K. J. (2005), *"Hemodynamic correlates of EEG:A heuristic"*, NeuroImage 28, 280–286.

[15] Goldman, R. I., Stern, J. M., Engel, J., Cohen, M. S., (2002), *"Simultaneous EEG and fMRI of the alpha rhythm*", NeuroReport 13, 2487–2492.

[16] Koch, S. P., Steinbrink, J., Villringer, A., Obrig, H., (2006), *"Synchronisation between background activity adn visually evoked potential is not mirrored by focal hyperoxygenation: Implications for the interpretation of vascular brain imaging",* Journal of Neuroscience 26, 4940–4948.

[17] Scheeringa, R., Petersson, K. M., Oosten- veld, R., Norris, D. G., Hagoort, P., Bastiaansen, M. C. M., (2009), *"Trial-by-trial coupling between EEG and BOLD identifies networks related to alpha and theta EEG power increases during working memory maintance",* Neuroimage 44, 1224–1238.

[18] Ritter, P., Villringer, A., (2006), *"Review: Simultaneous EEG-fMRI",* Neuroscience and Biobehavioral Reviews 30, 823–838.

[19] Lemieux, L., Allen, P. J., Franconi, F., Symms, M. R., Fish, D. R., (1997) *"Recording of EEG during fMRI experiments: Patient safety",* Magnetic Resonance in Medical Science 38, 943–952.

[20] Jorge J., Grouiller F., Ipek Ö., Stoermer R., Michel C.M., Figueiredo P., Zwag W., Gruetter R., (2015), *"Simultaneous EEG-fMRI at ultra-high field: Artifact prevention and safety assessment",* NeuroImage 105, 132-144.

[21] K. J. Mullinger, Castellone P., Bowtell R., (2013) *"Best current practice for obtaining high quality EEG data during simultaneous fMRI",* Journal of Visualized Experiments 76.

[22] Müri R., Felblinger J., Rosler K., Jung B., Hess C., Boesch C., (1998) *"Recording of electrical brain activity in a magnetic resonance environment: Distorting effects of the static magnetic field"*, Magnetic Resonance in Medicine 39, 18-22.

[23] Anami K., Mori T., Tanaka F., Kawagoe Y., Okamoto J., Yarita M., Ohnishi T., Yumoto M., Matsuda H., Saitoh O., (2003), *"Stepping stone sampling for retrieving artifact-free electroencephalogram during functional magnetic resonance imaging",* NeuroImage 19, 281-295.

[24] Allen P. J., Josephs O., Turner R., (2000) *"A method for Removing Imaging Artifact from Continuous EEG Recorded during Functional MRI",* NeuroImage 12, 230-239.

[25] Niazy R. K., Bechmann C. F., Iannetti G. D., Brady J. M., Smith S. M., (2005), *"Removal of fMRI environment artifacts from EEG data using optimal basis sets",* NeuroImage 28, 720-737.

[26] Bonmassar G., Purdon P.L, Jääakeläinen I.P., Chiappa K., Solo V., Brown E.N. Belliveau J.W. (2001), *"Motion and Ballistocardiographic artifact removal for interleaved recording of EEG and EPs during MRI",* NeuroImage 16, 1127-1141.

[27] Yan W. X., Mullinger K. J., Geirsdottir G. B., Bowtell R., (2010),*"Physical Modeling of Pulse Artefact Sources in Simultaneous EEG/fMRI",* Human Brain Mapping 31, 604-620.

[28] Mullinger K. J., Havenhand J., Bowtell R., (2013), *"Identifying the sources of the pulse artefact in EEG recordings made inside an MR scanner",* NeuroImage 71, 75-83.

[29] Debener S., Mullinger K. J., Niazy R. K., Bowtell R. W., (2008), *"Properties of the ballistocardiogram artefact as revealed by EEG recording at 1.5, 3 and 7 T static magnetic filed strength",* International Journal of Psychophysiology 67, 189-199.

[30] Allen P. J., Polizzi G., Krakow K., Fish D.R., Lemieux L., (1998), *"Identification of EEG events in the MR scanner: the problem of pulse artifact and a method for its subtraction"*, NeuroImage 8, 229-239.

[31] Debener, S., Strobel, A., Sorger, B., Peters, J., Kranczioch, C., Engel, A.K., Goebel, R., (2007), *"Improved quality of auditory event-related potentials recorded simultaneously with 3-T fMRI: removal of the ballistocardiogram artefact".* NeuroImage 34, 590–600.

[32] Vanderperren K., De Vos M., Ramautar J.R., Novitskiy N., Mennes M. Assecondi S., Vanrumste B., Stiers P., Van den Bergh B.R.H., Wagemans J., Lagae L., Sunaert S., Van Huffel S., (2010), *"Removal of BCG artifacts from EEG recordings inside the MR scanner: A comparison of methodological and validation-related aspects",* NeuroImage 50, 920-934.

[33] Srivastava G., Crottaz-Herbette S., Lau K. M., Glover G. H, Menon V., (2005), *"ICA-based procedures for removing ballistocardiogram artifacts from EEG data acquired in the MRI scanner",* NeuroImage 24, 50-60.

[34] Mantini D., Perrucci M.G., Cugini S., Ferretti A., Romani G. L. Del Gratta C., (2007), *"Complete artifact removal for EEG recorded during continuous fMRI using independent component analysis",* NeuroImage 34, 598-607.

[35] Debener, S., Ullsperger, M., Siegel, M., Fiehler, K., von Cramon, D.Y., Engel, A.K.,

(2005). "*Trial-by-trial coupling of concurrent electroencephalogram and functional magnetic resonance imaging identifies the dynamics of performance monitoring",* Journal of Neuroscience 25, 11730–11737.

[36] Delorme A., Makeig S., (2003), *"EEGLAB: an open source toolbox for analysis of signal-trial EEG dynamics including independent component analysis"*, Journal of Neuroscience Methods 134, 9-21.

[37] Liu Q., Balsters J.H., Baechinger M., Groen O., Wenderoth N., Mantini D., (2015), *"Estimating a neutral reference for electroencephalographic recordings: the importance of using a high-density montage and a realistic head model",* Journal of Neural Engineering 12.

[38] Iannotti G.R., Pittau F., Michel C.M., Vulliemoz S., Grouiller F., (2015), *"Pulse artefact detection in simultaneous EEG-fMRI recording based on EEG map topography",* Brain Topography 28, 21-32.

[39] J.W. Tukey, (1977) *"Exploratory Data Analysis, Addison-Wesley",* Reading, MA

Appendix – Matlab script

```
%% R peaks detection

ecg = D(ecg_channel,:);
ecg = net_fir_hanning(ecg,Fs,5,20);
ecg(1:fix(minpeakdistance/2)) = 0;
ecg(ntp-fix(minpeakdistance/2):ntp) = 0;

  if prctile(ecg,1)+prctile(ecg,99)<0
     ecg = -ecg;
  end

ecg = (ecg-mean(ecg))/std(ecg);

minpeakdistance = 600;
minpeakheight = 1.5;

[pks_ecg,locs_ecg] =
findpeaks(ecg,'minpeakheight',minpeakheight,'minpeakdistance',minpeakdistance);



%% Cz referred signal construction and BCG detection

ref = 0-mean( eeg_data,1);

ref = net_fir_hanning(ref,Fs,5,20);
ref(1:fix(minpeakdistance/2)) = 0;
ref(ntp-fix(minpeakdistance/2):ntp) = 0;
ref = (ref-mean(ref))/std(ref);

bcg = ref;

[c,lags] = xcorr(bcg,ecg,300,'coeff');
[max_c,I] = max(c);
globa_delay = lags(I);

PArange=600;

for kk = 1:nbeats-1

   disp(kk)
   bcg_tmp = bcg(locs_ecg(kk):locs_ecg(kk)+PArange);
   bcg_tot(kk,:) = bcg_tmp;

end

bcg_tot_ave = mean(bcg_tot);

for kk = 1:nbeats-1
```

```
    disp(kk)
    bcg_tmp = bcg_tot(kk,:);
    [pks_tmp,locs_tmp] = findpeaks(bcg_tmp(abs(delay)-30:abs(delay)+30));

    if isempty(locs_tmp)

        [pks_tmp,locs_tmp] = findpeaks(bcg_tot_ave(abs(delay)-30:abs(delay)+30));
    end

    locs_tmp = locs_tmp+abs(delay)-30-1;

    locs_bcg(kk) = locs_ecg(kk)+locs_tmp;

    locs_tmp_tot(kk) = locs_tmp;

    pks_bcg(kk) = pks_tmp;

end
```

%% statistical analysis of RR interval R-BCG delay

```
delay_R_BCG = locs_bcg-locs_ecg(1:end-1);

RR_interval = diff(locs_ecg);

 x=[delay_R_BCG];
k=1.5;
[Q1 Q3 outlier] = Tukey_method(x',k);

new_RR_interval=RR_interval;
new_RR_interval(outlier)=[];
new_delay_R_BCG=delay_R_BCG;
new_delay_R_BCG(outlier)=[];

new_corr_ecg_bcg_tw = corr(new_diff_ecg_bcg',new_diff_ecg','type','Pearson');
```

%% epoching of EEG signals using ECG peaks

```
for ch = 1:nchan
    disp(ch)
    eegchan_tmp = eeg_data(ch,:)-mean(eeg_data,1);

    for kk = 1:nbeats

        epoched_tmp = eegchan_tmp(locs_ecg(kk):locs_ecg(kk)+PArange);
        epoched_tot(kk,:) = epoched_tmp;

    end
   mean_tmp = mean(epoched_tot);
  mean_epoched_tot(ch,:) = mean_tmp;

end
```

```
%% Evaluation of RMS

% performed for each subject

root_mean_square = rms(mean_epoched_tot);


%% cross-correlation between signals of subject 2 and other subjects

% it is performed for every subject
epoched_data_reference_subject=mean_epoched_2';

epoched_data_other_subject=mean_epoched_tot';

nsamples = 600;

reference_peak_1 = 146;
reference_peak_2 = 219;
reference_peak_3 = 282;
reference_peak_4 = 417;
reference_peak_5 = 454;


for i = 1:nsamples

R=corrcoef(epoched_data_reference_subject(reference_peak_1,:),epoched_data_other_subject(i
,:));
    R_tot(i) = R(2);

end

[corr l_corr]=max(R_tot);

%values obtained by cross-correlation

inst_1=[147 146 177 125 131 135];
inst_1_mean=mean(inst_1);
inst_2=[226 219 193 262 231 221];
inst_2_mean=mean(inst_2);
inst_3=[263 282 271 292 302 294];
inst_3_mean=mean(inst_3);
inst_4=[411 417 374 420 369 413];
inst_4_mean=mean(inst_4);
inst_5=[524 454 538 441 481 558];
inst_5_mean=mean(inst_5);


%% normalization of average EEG signals

xb1=mean_epoched_tot;
xb2=mean_epoched_tot;
xb3=mean_epoched_tot;
xb4=mean_epoched_tot;
xb5=mean_epoched_tot;
```

```
xb6=mean_epoched_tot;

x=xb1;
y_eeg_1_norm = 2*(x - min(x(:)))/(max(x(:)) - min(x(:))) - 1;
x=xb2;
y_eeg_2_norm = 2*(x - min(x(:)))/(max(x(:)) - min(x(:))) - 1;
x=xb3;
y_eeg_3_norm = 2*(x - min(x(:)))/(max(x(:)) - min(x(:))) - 1;
x=xb4;
y_eeg_4_norm = 2*(x - min(x(:)))/(max(x(:)) - min(x(:))) - 1;
x=xb5;
y_eeg_5_norm = 2*(x - min(x(:)))/(max(x(:)) - min(x(:))) - 1;
x=xb6;
y_eeg_6_norm = 2*(x - min(x(:)))/(max(x(:)) - min(x(:))) - 1;
```

%% creation of average maps

```
%map inst 1
for i=1:6
   eeg_1(i,:)=xb(:,inst_1(i),i);
end

mean_eeg_1=mean(eeg_1);

%map inst 2
for i=1:6
   eeg_2(i,:)=xb(:,inst_2(i),i);
end

mean_eeg_2=mean(eeg_2);

%map inst 3
for i=1:6
   eeg_3(i,:)=xb(:,inst_3(i),i);
end

mean_eeg_3=mean(eeg_3);

%map inst 4
for i=1:6
   eeg_4(i,:)=xb(:,inst_4(i),i);
end

mean_eeg_4=mean(eeg_4);

%map inst 5
for i=1:6
   eeg_5(i,:)=xb(:,inst_5(i),i);
end

mean_eeg_5=mean(eeg_5);

elecs = readlocs('256.sfp');
```

```
for j = 1:256
    chanpos(j,:) = [elecs(1,j).X,elecs(1,j).Y,elecs(1,j).Z];
end


x=mean_eeg_1;
y_eeg_1 = 2*(x - min(x(:)))/(max(x(:)) - min(x(:))) - 1;
x=mean_eeg_2;
y_eeg_2 = 2*(x - min(x(:)))/(max(x(:)) - min(x(:))) - 1;
x=mean_eeg_3;
y_eeg_3 = 2*(x - min(x(:)))/(max(x(:)) - min(x(:))) - 1;
x=mean_eeg_4;
y_eeg_4 = 2*(x - min(x(:)))/(max(x(:)) - min(x(:))) - 1;
x=mean_eeg_5;
y_eeg_5 = 2*(x - min(x(:)))/(max(x(:)) - min(x(:))) - 1;


%% PCA

 maps=[y_eeg_1; y_eeg_2; y_eeg_3; y_eeg_4; y_eeg_5];

d = maps';

[Q,P]=size(d);

[coeff, score, latent] = pca(d);

latent = latent/sum(latent)*100;


figure
ft_plot_topo3d(chanpos,score(:,1)); caxis([-1 1]);
hold on
plot3(chanpos(:,1),chanpos(:,2),chanpos(:,3),'k.')
title('First Component')

figure
ft_plot_topo3d(chanpos,score(:,2)); caxis([-1 1]);
hold on
plot3(chanpos(:,1),chanpos(:,2),chanpos(:,3),'k.')
title('Second Component')

figure
ft_plot_topo3d(chanpos,score(:,3)); caxis([-1 1]);
hold on
plot3(chanpos(:,1),chanpos(:,2),chanpos(:,3),'k.')
title('Third Component')

%% reconstruction maps

average = mean(d);

%reconstruction using PC1
```

```
maps_reconstr_PC1=score(:,1)*coeff(:,1)'+repmat(average,Q,1);

x=maps_reconstr_PC1;
y_reconstr_PC1 = 2*(x - min(x(:)))/(max(x(:)) - min(x(:))) - 1;

figure
ft_plot_topo3d(chanpos,y_reconstr_PC1); caxis([-0.5 0.5]);
hold on
plot3(chanpos(:,1),chanpos(:,2),chanpos(:,3),'k.')


%reconstruction using PC2
maps_reconstr_PC2=score(:,2)*coeff(:,2)'+repmat(average,Q,1);

x=maps_reconstr_PC2;
y_reconstr_PC2 = 2*(x - min(x(:)))/(max(x(:)) - min(x(:))) - 1;

figure
ft_plot_topo3d(chanpos,y_reconstr_PC2); caxis([-0.5 0.5]);
hold on
plot3(chanpos(:,1),chanpos(:,2),chanpos(:,3),'k.')
```